https://doi.org/10.5194/cp-2019-166
Preprint. Discussion started: 14 January 2020

Climate of the Past Discussions

Stripping back the Modern to reveal Cretaceous climate and temperature gradient underneath

Marie Laugié[1], Yannick Donnadieu[1], Jean-Baptise Ladant[2], Mattias Green[3], Laurent Bopp[4,5] and François Raisson[6].

[1]Aix Marseille Univ, CNRS, IRD, INRA, Coll. France, CEREGE, Aix-en-Provence, France
[2]Department of Earth and Environmental Sciences, University of Michigan, Ann Arbor, MI, USA
[3]School of Ocean Sciences, Bangor University, Menai Bridge, UK
[4]Ecole Normale Supérieure (ENS Paris) - Département des Géosciences - France
[5]Laboratoire de Météorologie Dynamique (UMR 8539) (LMD) - Université Pierre et Marie Curie - Paris 6, Institut national des sciences de l'Univers, École Polytechnique, École des Ponts ParisTech, Centre National de la Recherche Scientifique : UMR8539, École Normale Supérieure - Paris - France
[6]Total EP – R&D Frontier Exploration - France

ABSTRACT

During past geological times, the Earth suffered several intervals of global warmth but their driving factors remain equivocal. A careful appraisal of the main processes involved in those past events is essential to evaluate how they can inform future climates, and thus to provide decision makers with a clear understanding of the processes at play in a warmer world. In this context, the greenhouse Earth of the Cretaceous era, specifically the Cenomanian-Turonian (~94 Ma), is of particular interest, as it corresponds to a thermal maximum. Here we use the IPSL-CM5A2 Earth System Model to unravel the forcing parameters of the Cenomanian-Turonian greenhouse climate. We perform six simulations with an incremental change in five major boundary conditions in order to isolate their respective role on climate change between the Cretaceous and the preindustrial. Starting with a preindustrial simulation, we implement: (1) the absence of polar ice sheets, (2) the increase in atmospheric pCO_2 to 1120 ppm, (3) the change of vegetation and soil parameters, (4) the 1% decrease in the Cenomanian-Turonian value of the solar constant and (5) the Cenomanian-Turonian paleogeography. Between the first (preindustrial) simulation and the last (Cretaceous) simulation, the model simulates a global warming of more than 11°C. Most of this warming is driven by the increase in atmospheric pCO_2 to 1120 ppm. Paleogeographic changes represent the second major contributor to the global warming while the reduction in the solar constant counteracts most of the geographically-driven global warming. We also demonstrate that the implementation of Cretaceous boundary conditions flattens the temperature gradients compared to the piControl simulation. Interestingly, we show that paleogeography is the major driver of the flattening in the low- to mid-latitudes whereas the pCO_2 rise and polar ice sheet retreat dominate the high-latitudes response.

https://doi.org/10.5194/cp-2019-166
Preprint. Discussion started: 14 January 2020

Climate of the Past Discussions

1. INTRODUCTION

The Cretaceous era is of particular interest to understand the drivers of past greenhouse climates because of its prolonged episode of global warmth (O'Brien et al. 2017, Huber et al. 2018), specifically during the thermal maximum of the Cenomanian-Turonian (CT) interval (94 Ma). Proxy-based reconstructions and model simulations of sea-surface temperatures (SST) for the CT reveal that equatorial Atlantic was 4-6° warmer than today (Bice et al., 2006; Norris et al., 2002; Pucéat et al., 2007; Tabor et al., 2016) or even more (6-9° - Forster et al., 2007) during the Oceanic Anoxic Event 2 (OAE2). This is a short and abrupt episode of major climatic, oceanographic and global carbon cycle perturbations occurring at the CT Boundary and superimposed on the long-term global warmth (Jenkyns, 2010). High latitudes were also much warmer than today (Herman and Spicer, 2010; Spicer and Herman, 2010), as was the deep-sea with bottom temperatures reaching up to 20°C during the CT (Friedrich et al., 2012; Huber et al., 2002; Littler et al., 2011). Atmospheric temperatures were also very high as revealed by paleobotanical studies (Herman and Spicer, 1996) with high latitudes temperatures up to 17°C higher than today (Herman and Spicer, 2010) and possibly reaching annual means of 10-12°C in Antarctica (Huber et al., 1999). The steepness of the equator-to-pole gradients is still a matter of debate, in particular because of inconsistencies between data and models as the latter usually predict steeper equator-to-pole gradients (Barron, 1993; Heinemann et al., 2009; Huber et al., 1995; Tabor et al., 2016). Models and data generally agree, however, about a flattened SST gradient relative to today (Huber et al., 1995; Jenkyns et al., 2004; O'Brien et al., 2017; Robinson et al., 2019; Sellwood et al., 1994).

The main factor generally considered as responsible for the Cretaceous global warmth is the higher level of atmospheric CO_2 (Barron et al., 1995; Crowley and Berner, 2001; Foster et al., 2017; Royer et al., 2007). Several studies have aimed at reconstructing Cretaceous pCO_2 using various techniques, for instance based on the analysis of paleosols $\delta^{13}C$ (Hong and Lee, 2012; Leier et al., 2009; Sandler and Harlavan, 2006), liverworts $\delta^{13}C$ (Fletcher et al., 2006) or phytane $\delta^{13}C$ (Van Bentum et al., 2012; Damsté et al., 2008) or on leaf stomata analysis (Barclay et al., 2010; Mays et al., 2015). Modelling studies have also widely investigated the conundrum of Cretaceous pCO_2 question (Barron et al., 1995; Berner, 2006; Bice et al., 2006; Monteiro et al., 2012; Poulsen et al., 2001, 2007) in an attempt to refine the wide range obtained from the data (<900 to >5000 ppm). The typical atmospheric pCO_2 concentration resulting from these studies for the CT averages around a long-term value of 1120 ppm (Barron et al., 1995; Bice and Norris, 2003; Royer, 2013; Wang et al., 2014) which is equivalent to four times the preindustrial value (280 ppm = 1 P.A.L) . The pCO_2 level is however known to vary on shorter timescales

https://doi.org/10.5194/cp-2019-166
Preprint. Discussion started: 14 January 2020


Climate of the Past Discussions

during this period, in particular during OAE2, which may have been caused by a large increase in atmospheric pCO2, possibly reaching 2000 ppm or even higher, and which could be attributed to large igneous provinces volcanic activity (Jenkyns, 2010; Kerr and Kerr, 1998; Turgeon and Creaser, 2008). Proxy records suggest that the atmospheric CO_2 may then have dropped down to 900 ppm after carbon sequestration into organic-rich marine sediments (Van Bentum et al., 2012).

Paleogeography is also considered as a major driver of climate change through geological times (Crowley et al., 1986; Goddéris et al., 2014; Gyllenhaal et al., 1991; Lunt et al., 2016). Several processes linked to paleogeographic changes have been shown to impact the Cretaceous climate. This includes albedo and evapotranspiration feedbacks from paleovegetation (Otto-bliesner and Upchurch, 1997), seasonality due to continental break-up or presence of epicontinental seas (Fluteau et al., 2007), atmospheric feedbacks due to water cycle modification (Donnadieu et al., 2006), Walker and Hadley cells changes after Gondwana break-up (Ohba and Ueda, 2011) or oceanic circulation changes due to gateways opening (Poulsen et al., 2001, 2003). Other potential controlling factors include the solar constant, which has been shown to change through time (Gough et al. 1981) and whose impact on Cretaceous climate evolution was quantified by Lunt et al. (2016), and changes in the distribution of vegetation, which has been suggested to drive warming, especially in the high-latitudes with a temperature increase of up to 4°-10°C in polar regions (Brady et al., 1998; Deconto et al., 2000; Hunter et al., 2013; Otto-bliesner and Upchurch, 1997; Upchurch, 1998).

Despite all these studies, there is no established consensus on the relative importance of these controlling factors on the CT climate. In particular, the primary driver of Cretaceous climate has suggested to be either pCO_2 or paleogeography. Early studies suggested a negligible role of paleogeography on global climate compared to the high CO_2 concentrations (Barron et al., 1995) whereas others suggested that CO_2 was not the primary control (Veizer et al., 2000), or that the impact of paleogeography on climate was as important as a doubling of pCO_2 (Crowley et al., 1986)s. More recent modeling work has also suggested that paleogeographic changes could affect global climate (Donnadieu et al., 2006; Fluteau et al., 2007; Poulsen et al., 2003) and the latest work using coupled climate models are still divided on the climatic impact of paleogeography (Ladant and Donnadieu, 2016; Lunt et al., 2016; Tabor et al., 2016). For instance, Lunt et al. (2016) support a significant role of paleogeography at the regional rather than global scale and even show that the global paleogeographic signal is completely cancelled by an opposite trend due to solar constant changes. Tabor et al. (2016) also support an important regional climatic impact of paleogeography but argue that CO_2 is the main responsible for the Late

https://doi.org/10.5194/cp-2019-166
Preprint. Discussion started: 14 January 2020


Climate of the Past Discussions

Cretaceous climate evolution. In contrast, Ladant and Donnadieu (2016) find a significant impact of paleogeography on the mean global Late Cretaceous temperatures, roughly comparable to a doubling of atmospheric pCO_2. Finally, the role of paleovegetation is also uncertain since some studies show a major role at high-latitude (Hunter et al., 2013; Upchurch, 1998) whereas more recent work demonstrates limited impact at high latitudes (<2°C), with a cooling effect at low latitudes, under high pCO_2 values (Zhou et al., 2012).

In this study, we investigate the forcing parameters of the CT greenhouse climate by using a set of simulation run with the IPSL-CM5A2 Earth System Model. We performed six simulations, from the preindustrial to the Cretaceous, and incrementally implement one additional boundary condition change among the following: (1) the absence of polar ice sheets, (2) the increase in pCO_2 to 1120 ppm, (3) the change of vegetation and soil parameters, (4) the 1% reduction in the value of the solar constant and (5) the Cenomanian-Turonian paleogeography. We particularly focus on the processes driving warming or cooling of the atmospheric surface temperature under each boundary condition change in order to study the relative importance of each parameter in the Cenomanian-Turonian to preindustrial climate change. We also investigate how the SST gradient responds to boundary condition changes in order to understand the evolution of its steepness between the Cretaceous and the present.

2. MODEL DESCRIPTION & EXPERIMENTAL DESIGN

2.1 IPSL-CM5A2 MODEL

IPSL-CM5A2 is an updated version of the IPSL-CM5A-LR earth system model developed at the IPSL (Institut Pierre-Simon Laplace) as part of the CMIP5 (Dufresne et al., 2013). It is a coupled Earth system model capable of simulating interactions between atmosphere, ocean and sea ice, and land surface. It also includes the marine carbon and other key biogeochemical cycles (C, P, N, Fe and Si - See Aumont et al., 2015). IPSL-CM5A has a rich history of applications, including present-day and future climates (Aumont and Bopp, 2006; Swingedouw et al., 2017), the IPCC AR5 exercise and CMIP5 project (Dufresne et al., 2013), preindustrial studies (Gastineau et al., 2013) and paleoclimate (Bopp et al., 2017; Contoux et al., 2015; Kageyama et al., 2013; Sarr et al., 2019; Tan et al., 2017). IPSL-CM5A has also been used to explore the links between marine productivity and climate (Bopp et al., 2013; Ladant et al., 2018; Le Mézo et al., 2017), vegetation and climate (Contoux et al., 2013; Woillez et al., 2014) or topography and climate (Maffre et al., 2018), but also the role of nutrients in the global carbon cycle (Tagliabue et al., 2010) or the variability of the oceanic circulation and upwelling (Ortega et al., 2015; Swingedouw et al., 2015). Following technical developments on the components of IPSL-CM5A described in

https://doi.org/10.5194/cp-2019-166
Preprint. Discussion started: 14 January 2020


Climate of the Past Discussions

Sepulchre et al. (2019), the new IPSL-CM5A2 model provides enhanced computing performances allowing long thousand-years long integrations required for deep-time paleoclimate applications or long-term future projections.

In details, IPSL-CM5A2 is composed of the LMDz atmospheric model (Hourdin et al., 2013), the ORCHIDEE land surface and vegetation model (continental hydrological cycle, vegetation, carbon cycle; Krinner et al., 2005) and the NEMO ocean model (Madec, 2012) including the LIM2 sea-ice model (Fichefet and Maqueda, 1997) and the PISCES marine biogeochemistry model (Aumont et al., 2015). The OASIS coupler (Valcke et al., 2006) ensures a good synchronization of the different components and the XIOS input/output parallel library is used to read and write data. The LMDZ atmospheric component has a horizontal resolution of 96x95, (equivalent to 3.75° in longitude and 1.875° in latitude) and 39 uneven vertical levels. ORCHIDEE shares the same horizontal resolution whereas NEMO – the ocean component – has 31 uneven vertical levels (from 10 meters at the surface to 500 meters at the bottom), and a horizontal resolution of approximately 2°, enhanced to up to 0.5° in latitude in the tropics. NEMO uses the ORCA2.3 tripolar grid to overcome the North Pole singularity (Madec and Imbard, 1996). IPSL-CM5A2 and its performances in simulating preindustrial and modern climates are fully described in Sepulchre et al. (2019).

2.2 EXPERIMENTAL DESIGN

Six simulations have been performed for this study: one preindustrial control simulation named *piControl* and five simulations for which boundary conditions were changed incrementally to progressively reconstruct the Cretaceous conditions (Table 1): (1) *1X-NOICE* with polar ice caps retreat, *4X-NOICE* (pCO_2 at 1120 ppm), *4X-NOICE-PFT-SOIL* (implementation of idealized Plant Functional Types (PFTs) and mean parameters for soil), *4X-NOICE-PFT-SOIL-SOLAR* (reduction of the solar constant) and *4X-CRETACEOUS* (CT paleogeography). The piControl simulation was run for 1800 years and the five others for 2000 years in order to reach the equilibrium state (Fig.1).

The piControl and 1X-NOICE simulations are initialized with Atmospheric Model Intercomparison Project (AMIP) conditions that were constrained by realistic sea surface temperature (SST) and sea ice from 1979 to near present (Gates et al., 1999). Modern boundary conditions of NEMO include forcings of the dissipation associated with internal wave energy for the M2 and K1 tidal components (de Lavergne et al., 2019). The parameterization follows Simmons et al. (2004) with refinements in the modern Indonesian Through Flow (ITF) region according to Koch-Larrouy et al. (2007). As most evidence suggests the absence of permanent polar ice sheets during the CT

https://doi.org/10.5194/cp-2019-166
Preprint. Discussion started: 14 January 2020


Climate of the Past Discussions

(Huber et al., 2018; Ladant and Donnadieu, 2016; MacLeod et al., 2013), we isostatically remove polar ice sheets in the 1X-NOICE simulation and replace them with brown bare soil. In the 4X-NOICE simulation, polar ice caps are also removed and the $pCO_{2\,is}$ fixed to 1120 ppm (four times the "Preindustrial Atmospheric Level" [P.A.L]), a value reasonably close to the mean suggested by a recent compilation of Cretaceous pCO_2 reconstructions (Wang et al., 2014). In an attempt to reach the equilibrium state faster, the initial conditions of simulations with 4x PAL are taken from idealized conditions (higher SST and no sea ice) similar to those described in Lunt et al., 2017. We keep the 13 PFTs of ORCHIDEE but their distribution is reassigned along latitudinal bands, based on a rough comparison with the preindustrial distribution of vegetation, in order to obtain a theoretical latitudinal distribution usable for any geological period. The list of PFTs and associated latitudinal distribution and fractions are described in the Supplementary Table 1. The soil parameters, i.e., the mean color and texture (rugosity), are calculated from preindustrial maps (Wilson and Henderson-sellers, 2003; Zobler, 1999) and assigned to the whole world. The impact of these idealized PFTs and mean parameters is discussed in the results. The 4X-NOICE-PFT-SOIL-SOLAR is initialized from the same conditions as 4X-NOICE-PFT-SOIL except that the solar constant is reduced to its Cretaceous value (Gough, 1981). We use here the value of 1351.36 W/m^2 (98.9% of the Modern solar luminosity, calculated for an age of 90 My). Finally, the 4X-CRETACEOUS simulation incorporates the previous modifications plus the implementation of the CT paleogeography. The land-sea configuration used here is the one proposed by Sewall (2007) for the CT, in which we have implemented the bathymetry from Müller (2008) (Fig. 2). These bathymetric changes are done in order to represent deep oceanic topographic features, such as ridges, that are absent from the Sewall paleogeographic configuration. In this simulation, the mean soil color and rugosity as well as the theoretical latitudinal PFTs distribution are adapted to the new land-sea mask and the river routing is recalculated from the new topography. To create a cenomanian-turonian dissipation forcing, we used a M2 tidal field calculated using the Oregon State University Tidal Inversion System (OTIS, Egbert et al., 2004; Green and Huber, 2013). The M2 field is computed using our cenomanian-turonian bathymetry and an ocean stratification taken from an equilibrated cenomanian-turonian simulation realized with the IPSLCM5A2 with no M2 field. In the absence of any estimation for the Cretaceous, we prescribe the K1 tidal field to 0. In addition, the parameterization of Koch-Larrouy et al. (2007) is not used here because the ITF does not exist in the Cretaceous.

https://doi.org/10.5194/cp-2019-166
Preprint. Discussion started: 14 January 2020

Climate of the Past Discussions
Open Access
EGU

175 *Table 1 : Description of the simulations. The parameters in bold indicate the specific change for the corresponding simulation. Simulations are run for 2000 years, except piControl which is run*
176 *for 1000 years.*

177

Simulation	piControl	1X-NOICE	4X-NOICE	4X-NOICE-PFT-SOIL	4X-NOICE-PFT-SOIL-SOLAR	4X-CRETACEOUS
Polar Caps	Yes	**No**	No	No	No	No
CO_2 (ppm)	280	280	**1120**	1120	1120	1120
Vegetation	IPCC (1850)	IPCC (1850) + Bare soil instead of polar caps	IPCC (1850) + Bare soil instead of polar caps	**Theoretical latitudinal PFTs**	Theoretical latitudinal PFTs	Theoretical latitudinal PFTs
Soil Color/Texture	IPCC (1850)	IPCC (1850) + Brown soil instead of polar caps	IPCC (1850) + Brown soil instead of polar caps	**Uniform mean value**	Uniform mean value	Uniform mean value
Solar constant (W/m^2)	1365.6537	1365.6537	1365.6537	1365.6537	**1353.36**	1353.36
Geographic configuration	Modern	Modern	Modern	Modern	Modern	**Cretaceous 90 Ma (Sewall 2007 + Müller 2008)**

178

https://doi.org/10.5194/cp-2019-166
Preprint. Discussion started: 14 January 2020

Climate of the Past Discussions
Open Access
EGU

3. RESULTS

The simulated changes between the preindustrial simulation (piControl) and the Cretaceous simulation (4X-CRETACEOUS) can be decomposed into five components: (1) Polar cap retreat (Δice), (2) pCO_2 (ΔCO_2), (3) PFT and Soil parameters (ΔPFT-SOIL), (4) Solar constant (Δsolar) and (5) Paleogeography (Δpaleo). Each contribution on global climate change can be calculated by a linear factorization (Broccoli and Manabe, 1987; Von Deimling et al., 2006), which simply corresponds to the anomaly between two consecutive simulations. The results presented in the following are averages calculated over the last 100 simulated years (out of 2000).

3.1 GLOBAL

The progressive change of parameters made to reconstruct Cretaceous climate induce a general global warming (Table 2, Fig. 3). The annual global atmosphere temperature at 2 meters above the surface (T2M) rises from 13.25°C to 24.35 °C, which represents an increase of 84%. The majority of this warming, 9°C or a contribution of 61% of the cumulative absolute temperature change between the preindustrial and the CT the signal, comes from increasing the pCO_2 to 4 P.A.L. The paleogeography also represents a major contributor to the warming, with an increase in T2M of 2.6°C (18%). The impact of the solar constant decrease contributes to 12% of change (1.8°C), but with an opposite effect of cooling. Finally, changes in the soil parameters and PFTs as well as the retreat of polar caps have a minor impact on the global T2M (6% and 3% change, respectively).

The temperature changes have a different geographic response (Fig. 4) depending on the changed parameter, ranging from a global and uniform cooling (Δsolar – Fig 4e) to a global warming (ΔpCO_2 – Fig 4c), via contrasted regional responses (Δice or Δpaleo – Fig 4b and 4f). In the next section, we describe the main patterns of change and the main feedbacks arising.

		piControl	1X-NOICE	4X-NOICE	4X-NOICE-PFT-SOIL	4X-NOICE-PFT-SOIL-SOLAR	4X-CRETACEOUS
T2M (°C)	Global Anomaly	+11.1 → +84%					
	Results	13.25	13.75	22.75	23.55	21.75	24.35
Planetary Albedo (%)	Global Anomaly	-5.94 → -18%					
	Results	33.07	32.61	28.79	28.27	28.66	27.13

https://doi.org/10.5194/cp-2019-166
Preprint. Discussion started: 14 January 2020

Surface Albedo (%)	Global Anomaly	-5.19 → -26%					
	Results	20.13	19.02	16.56	15.46	15.35	14.94
Emissivity (%)	Global Anomaly	-4.97 → -8%					
	Results	62.01	61.7	57.51	57.14	57.77	57.04

Table 2 : Simulations results (Global annual mean over last 10 years of simulation) and calculated anomaly between 4XCRETACEOUS and piControl simulations.

3.2 The major contributor to global warming - ΔCO_2

The fourfold increase in pCO_2 leads to a global warming of 9°C (Table 3, Fig. 3) between 1X-NOICE-and 4X-NOICE simulations. The whole surface is warmer with an amplification located over the Arctic and Austral oceans and which is generally larger over continents than over oceans (Fig 4c). The warming is due to a general decrease of planetary albedo and of the atmosphere's emissivity. The decrease in atmosphere's emissivity is directly driven by the increase of CO_2, and thus greenhouse trapping in the atmosphere, but it is also amplified by an increase in high-altitude cloudiness over the Antarctic continent (Fig 5a,b). The decrease in planetary albedo is due to (1) a decrease of sea ice and snow (especially over Northern hemisphere continents and along the coasts of Antarctica) and thus of surface albedo, which explain the warming amplification over polar oceans, and (2) a decrease in low-altitude cloudiness (except over the Arctic - Fig 5a,b). The decrease in low-altitude cloudiness is linked to a decrease of relative humidity in areas of formation of low clouds (outside of the tropics), despite a general increase of evaporation and specific humidity. The relative humidity decrease can be driven by the temperature rise associated with enhanced greenhouse trapping, allowing the atmosphere to hold more moisture. Over the Arctic, an increase in low-altitude cloudiness is simulated despite the decrease in relative humidity, and can be described by a strong sea level pressure decrease allowing more air to rise and more clouds to form. This sea level pressure decrease is possibly a feedback driven by the sea ice melting and associated higher temperatures. Here, the increase in low-altitude cloudiness acts as a negative feedback and attenuates the warming induced by the surface albedo decrease. Nevertheless, its impact is minor given the strong atmospheric temperature warming observed over the Arctic (Fig 4c).

The contrast in the response of the atmosphere over continents and oceans is due to the impact of the evapo-transpiration feedback. The warming drives an increase of evaporation, which acts as a negative feedback and moderates the warming by consuming more latent heat at the ocean surface. In contrast, high temperatures tend to inhibit vegetation development over continents, which

https://doi.org/10.5194/cp-2019-166
Preprint. Discussion started: 14 January 2020


Climate of the Past Discussions
Open Access
EGU

231 acts as positive feedback and enhances the warming due to reduced transpiration and reduced latent
232 heat consumption.
233

234 ### 3.3 Boundary conditions with the smallest global impacts – Δice, ΔPFT-SOIL, Δsolar

235 The polar cap retreat, in 1X-NOICE simulation, leads to a weak global warming of 0.5°C but a
236 strong regional warming observed over areas previously covered by ice caps (Antarctica and
237 Greenland – Fig 4a,b). This is due to a combination of a decrease in elevation and of surface albedo,
238 which is directly linked to the removal of polar ice sheets. Unexpected cooling is also simulated in
239 specific areas, such as the margins of the Arctic Ocean and the southwestern Pacific. These contrasted
240 climatic responses to the impact of ice sheets on sea surface temperatures have been observed in
241 previous modeling studies but their origin is still unclear (Goldner et al., 2014; Kennedy et al., 2015;
242 Knorr and Lohmann, 2014).
243 The change in soil parameters and the implementation of theoretical zonal PFTs, in simulation
244 4X-NOICE-PFT-SOIL, drive a warming of 0.8 °C. This warming is essentially located above arid areas,
245 such as the Sahara, Australia, or the Middle-East, and polar latitudes (Antarctica/Greenland) (Fig 4d).
246 The warming above arid areas is mostly caused by the implementation of a mean uniform soil color,
247 which drives a surface albedo decrease over deserts that normally have a lighter color. The warming at
248 high latitudes is linked to the vegetation change: the bare soil, that characterizes the continental
249 regions previously covered with ice, is replaced by boreal vegetation, which drives a surface albedo
250 decrease. The presence of vegetation at such high latitudes is consistent with high latitude
251 paleobotanical data ant temperature records during the Cretaceous (Herman and Spicer, 2010; Otto-
252 bliesner and Upchurch, 1997; Spicer and Herman, 2010).
253 Finally, the change in solar constant from 1365 W/m^2 to 1353 W/m^2 directly drives a cooling
254 of 1.8 °C, rather evenly distributed over the Earth (Fig 4e), see Gough (1981).
255

256 ### 3.4 The most complete response - Δpaleogeography

257 The paleogeographic change drives a global warming of 2.6 °C. This is seen all year round in
258 the Southern Hemisphere, while the Northern Hemisphere experiences a warming during winter and a
259 cooling during summer (Fig 6). These temperature changes are linked to a general decrease of
260 planetary albedo and/or emissivity, although the Northern Hemisphere experiences an increased
261 albedo, due to the increase in low-altitude cloudiness. This trend is compensated by a strong
262 atmosphere emissivity decrease during winter but not during summer, which leads to the seasonal
263 pattern of cooling and warming.

https://doi.org/10.5194/cp-2019-166
Preprint. Discussion started: 14 January 2020


Climate of the Past Discussions
Open Access
EGU

The albedo and emissivity changes are linked to atmospheric and oceanic circulation modifications driven by major features of the new paleogeography (Fig 2):

(1) Equatorial oceanic gateway opening (Panama/Tethys)
(2) Polar gateway closure (Drake/Tasman)
(3) Increase of oceanic area in the North Hemisphere (Fig 2)
(4) Decrease of oceanic area in the South Hemisphere (Fig 2)

The opening of equatorial gateway creates a zonal connection between the Pacific, Atlantic and Indian oceans via the Tethys. This connection allows a strong circumglobal equatorial current to form under the influence of stronger easterly winds because of the absence of continental barriers in the CT configuration (Fig 7a-b). These winds and currents drive an intensification of upwelling along the equator and of the surface meridional currents (Fig8a-b), and therefore an increased poleward ocean heat transport (Fig 8c) (Enderton and Marshall, 2008; Hotinski and Toggweiler, 2003). A similar line of reasoning can be used in the Southern Hemisphere to explain the increase of southward ocean heat transport observed between 40° and 60°S (Fig 8c). The modern Antarctic Circumpolar Current (ACC) does not exist during the Cretaceous because of the closed Drake and Tasman gateways (Fig 7c-d), and the ocean heat transport is thus enhanced. An altered circulation emerges in the Southern Ocean, showing a more gyre-like circulation, which allows and increased polar heat transport. The increased oceanic heat transport is associated with a meridional expansion of high sea-surface temperatures leading to an intensification of evaporation between the tropics and a shift of the ascending branches of the Hadley cells a few degrees off the Equator towards the subtropics. The combination of these two processes results in an increased injection of moisture into the upper atmosphere and thus in high-altitude cloudiness increase and spreading towards the tropics, leading to an important greenhouse effect. This process acts as the main factor of intertropical warming (Herweijer et al., 2005; Levine and Schneider, 2010; Rose and Ferreira, 2013).

The atmosphere response to paleogeographic change in the mid- and high-latitudes is different in the Southern and Northern Hemispheres as the oceanic areas decrease or increase between the CT configuration and the modern. In the Southern Hemisphere, the reduced ocean surface area (Fig 2) limits evaporation and moisture injection into the atmosphere, which in turn leads to a decrease in relative humidity and low-altitude cloudiness (Supplementary Fig 1) and an associated year-round warming due to a reduced planetary albedo. In the Northern Hemisphere, the oceanic area increases (Fig 2) and results in a strong increase of evaporation and moisture injection into the atmosphere. Low-altitude cloudiness and hence the albedo, both increase and lead to the cooling during the summer as discussed above (Fig 6). During winter, on the other hand, an increase of high-altitude cloudiness leads to an enhanced greenhouse effect and counteracts the larger albedo. This

https://doi.org/10.5194/cp-2019-166
Preprint. Discussion started: 14 January 2020


Climate of the Past Discussions
Open Access
EGU

high-altitude cloudiness increase is due to the extratropical increase in OHT (Fig. 8) which enhances mid-latitude convection and moist air injection into the upper troposphere which spreads towards the pole (see also Rose and Ferreira, 2013). Also, the increased continental fraction of the Cretaceous paleogeography leads to a decreased continentality (Donnadieu et al. 2006) because of the thermal inertia of the oceans that is different to that of continents.

3.5 Temperature Gradients

3.5.1 Ocean

The mean annual global SST increases of 9.8°C, from 17.9°C to 27.7 °C across the simulations. This warming is slightly weaker than the mean annual global atmospheric temperature at 2m discussed above, and most likely occurs because of evaporation processes due to the weaker atmospheric warming above oceans compared to that above continents. As for atmospheric temperatures, pCO_2 appears as the major controlling parameter of the ocean warming (49% of the absolute temperature change), followed by paleogeography (30%) and solar constant (16%), although the latter again drives cooling rather than warming. PFT and soil parameter changes and polar ice cap retreat instead have a minor impact at the global scale (4% and 0% respectively). It is interesting to note the increased contribution of paleogeography in the simulated sea surface warming compared to the atmospheric warming, which is probably driven by the major changes simulated in the surface circulation (Fig. 7).

The piControl simulation show an average tropical SST average of ~ 26°C (calculated as the zonal average between 30°S and 30°N) and of ~ -1.5°C at the poles (beyond 70° N - Fig 9a). The meridional temperature gradients, calculated as the linear temperature change per 1° of latitude between 30° and 80°, are of 0.45°C/°latitude and 0.44°C/°latitude for the Northern and Southern Hemispheres, respectively. The Cretaceous simulation yields SST averages of ~ 33.3°C in the tropics and of ~5°C and 10°C in the Arctic and Southern Ocean respectively. Associated Cretaceous meridional gradients are of 0.45°C/°latitude and 0.39°C/°latitude for the Northern and Southern Hemispheres, respectively. The progressive flattening of the SST gradient can be explained by superimposing the zonal mean temperatures of the different simulation and by adjusting them at the Equator (Fig 9b). Two major observations can be made from these results. First, paleogeography has a strong impact on the low-latitudes SST gradient because it widens the latitudinal band of relatively homogeneous warm tropical SST). As explained before (See Results – Δpaleogeography), this is due to the opening of equatorial gateways. Second, the SST gradient beyond 40° of latitude is flattened in two steps with paleogeography being the major contributor followed by atmospheric pCO_2 increase.

https://doi.org/10.5194/cp-2019-166
Preprint. Discussion started: 14 January 2020


Climate of the Past Discussions
Open Access
EGU

333 3.5.2 Atmosphere

334 In the piControl simulation, tropical atmospheric temperatures are ~ 23.6°C whereas polar
335 temperatures (calculated as the zonal average between 80° and 90° of latitude) in the Northern and
336 Southern Hemisphere are around -16.8°C and -37°C respectively. The northern meridional
337 temperature gradient is 0.69°C/°latitude while the southern latitudinal temperature gradient is
338 1.07°C/°latitude (Fig 9c). In the Cretaceous simulation, the tropical atmospheric temperatures are ~
339 32.3°C and polar temperatures ~ 3.4°C in the Northern Hemisphere and ~ - 0.5°C in the Southern
340 Hemisphere. This yields latitudinal temperature gradients of 0.49°C/°latitude and 0.54°C/°latitude,
341 respectively. As for the SST gradients, we normalized the curves so that temperatures at the Equator
342 are equal for each simulation (Fig 9d). This shows that the different mechanisms responsible for the
343 flattening of the gradients are different for each hemisphere. In the south, at high-latitudes, three
344 parameters contribute to reducing the equator-to-pole temperature gradient in the following order of
345 importance: retreat of polar ice caps is the most important, paleogeography and atmospheric pCO_2
346 increase. In contrast, in the Northern Hemisphere, only the rise in pCO_2 contributes to reducing the
347 steepness of the temperature gradient. Furthermore, in the Southern Hemisphere low- to mid-
348 latitudes, only the paleogeography acts to reduce the steepness of the temperature gradient, whereas
349 in the northern hemisphere low- to mid-latitudes, both paleogeography and atmospheric pCO_2
350 contribute to this decrease with a similar magnitude.

351 The role of the polar ice sheet retreat on gradient flattening is considerable but only locally
352 because of the geographic restriction of the ice sheets. We have seen that the removal of polar ice
353 sheets only warms areas initially covered by ice whereas equatorial temperatures remain unchanged
354 Fig. 4b). This explains the regionally flattened gradient in the Southern Hemisphere whereas the
355 smaller size of the Greenland ice sheet only marginally affects the northern gradient. In contrast, the
356 increase in pCO_2 exerts a more global impact that is amplified at high latitudes because of the sea ice
357 decrease. Finally, the contribution of paleogeography to the gradient flattening is observed almost at
358 all latitudes but is clearer in the Southern Hemisphere. In the tropics the impact of paleogeography on
359 the latitudinal atmospheric gradient is linked to the surface oceanic circulation changes described
360 previously. In the mid- to high-latitudes the increased continental areas in the Cretaceous Southern
361 Hemisphere drive the reduction in the steepness of the atmospheric gradient because of the
362 enhanced warming of continental areas. In the Northern Hemisphere, the increase in oceanic areas
363 instead tends to obscure the flattening of the atmospheric gradient.
364
365

https://doi.org/10.5194/cp-2019-166
Preprint. Discussion started: 14 January 2020

Climate of the Past Discussions
Open Access
EGU

4. DISCUSSION

4.1 ABOUT THE CENOMANIAN-TURONIAN CLIMATE

The results predicted by our CT simulation were compared to the reconstructed atmospheric and oceanic paleotemperatures from proxy data (Fig 10a,b). The SST data compilation is essentially based on that of Tabor (2016) and includes several proxies such as TEX86, $\delta^{18}O$ of fish teeth, foraminifera and shells, and crocodilian fossil evidence. Atmospheric temperature data are obtained from paleobotanical and paleosoil studies (see supplementary data for the complete database and references). Cretaceous equatorial and tropical SST have long been believed to be similar or even lower than those of today (Crowley and Zachos, 1999; Huber et al., 2002; Sellwood et al., 1994), thus feeding the problem of "tropical overheating" systematically observed in General Circulation Model simulations (Barron et al., 1995; Bush et al., 1997; Poulsen et al., 1998). This incongruence was based on the relatively low tropical temperatures reconstructed from foraminifera (25-30°C, Fig. 9a) but it has later been suggested that these were underestimated (Pearson et al., 2001; Pucéat et al., 2007). The latest data compilations including temperature reconstructions from other proxies (TEX86, $\delta^{18}O$ from shells or fish tooth) have provided support for high tropical SST in the Cenomanian-Turonian (O'Brien et al., 2017; Tabor et al., 2016) and our tropical SST are mostly consistent with existing paleotemperature reconstructions (Fig. 9a). In contrast to the numerous Cenomanian-Turonian SST records, there are, to our knowledge, no atmospheric temperature reconstructions available for tropical latitudes.

In the mid-latitudes (30-60°) the proxy records show a wide range of SST, ranging from 10°C to more than 30°C. We observe that this trend can be reproduced in our simulation when considering the local monthly maximum and minimum temperatures (grey shaded areas, Fig 10a), suggesting a reasonable model-data agreement. Simulated atmospheric temperatures for these latitudes in the Southern hemisphere also show reasonable agreement, whereas the Northern Hemisphere mean zonal temperatures in our model are slightly warmer than that inferred from proxies (Fig 10b).

There are unfortunately only a few high-latitudes SST data points available, which renders the model-data comparison difficult. This is further aggravated by both the proxy-based and simulated SST presenting a large range for a given latitude. In the Northern Hemisphere, temperatures inferred from the presence of crocodilian fossils (Vandermark et al., 2007) in the northern Labrador Sea (~70° of latitude, not represented in our paleogeography) are around 14°C for the annual mean and 5°C for the coldest month. In comparison, the simulated temperatures at the same latitude in the adjacent Western Interior Sea are very similar (13.5 °C for the annual mean and 7.9 °C for the coldest month). In the Southern Hemisphere, the mean annual SST calculated from foraminifera at sites DSDP 511 and 258 (Huber et al., 2018); 55° of latitude in our paleogeography) are between 25° and 30°C whereas

https://doi.org/10.5194/cp-2019-166
Preprint. Discussion started: 14 January 2020


Climate of the Past Discussions
Open Access
EGU

401 the simulated annual SSTs average at 14.2°C for this latitude. However, the simulated annual SSTs can
402 reach 19.4°C locally, with a monthly maximum up to 28°C, especially around the location of site DSDP
403 258. We speculate that a seasonal bias in the foraminiferal record may represent a possible cause for
404 this difference, as may local deviations of the regional seawater $\delta^{18}O$ from the globally assumed -1‰
405 value. The same trend is observed for atmospheric temperatures with data indicating higher
406 temperatures than the model at high latitudes for both southern and northern hemispheres.
407 However, we observe the same underestimate of simulated high-latitudes atmospheric temperatures
408 compared to observations in both hemispheres, which could indicate a systematic cool bias of the
409 simulated temperatures.
410 The simulated northern latitudinal SST gradient of (~0.45°C/°latitude) is in good agreement
411 with those obtained by geological data for the northern hemisphere (~0.42°C/°latitude) whereas the
412 simulated southern latitudinal gradient is significantly higher (~0.39°C/°latitude vs ~0.3°C/°latitude)
413 (Fig 11). This overestimate of the latitudinal gradient is also true for the atmosphere as data-inferred
414 gradients are much lower (North=0.2°C/°latitude, South=0.18°C/°latitude) than that of the simulation
415 (North=0.49°C/°latitude, South=0.55°C/°latitude), although the paucity of Cenomanian-Turonian
416 continental temperatures proxy data is likely to significantly bias this comparison.
417 In the following, we compare our simulated gradients to those obtained in previous deep time
418 modelling studies using recent earth system models. Because such modeling studies focusing on the
419 Cenomanian-Turonian are limited, we include simulations of the Early Eocene (~ 55 Ma), which is
420 another interval of global climatic warmth (Lunt et al., 2012a, 2017) (Fig. 11). The simulated SST
421 latitudinal gradients range from 0.32°C/°latitude to 0.55°C/°latitude (Lunt et al., 2012; Tabor et al.,
422 2016; Zhu et al., 2019; Fig. 11) and the atmospheric latitudinal gradients from 0.33°C/°latitude to
423 0.78°C/°latitude (Huber and Caballero, 2011; Lunt et al., 2012; Niezgodzki et al., 2017; Upchurch et al.,
424 2015; Zhu et al., 2019; See Fig. 11), with the lowest latitudinal gradients being obtained for the highest
425 pCO_2 values. The IPSL-CM5A2 is well within the range of other models, which almost systematically
426 simulate larger gradients than those obtained from data (Fig. 11, see also Huber, 2012). Reasons
427 behind this incongruence are debated (Huber, 2012) but it highlights the need to get more data and to
428 challenge the behavior of complex earth system models, in particular in the high latitudes. Studies
429 have demonstrated that models are able to simulate lower latitudinal temperature gradients under
430 specific conditions such as anomalously high CO_2 concentrations (Huber and Caballero, 2011),
431 modified cloud properties and radiative parameterizations (Upchurch et al., 2015; Zhu et al., 2019) or
432 lower paleo elevations and/or more extensive wetlands (Hay et al., 2019). Finally, from a proxy
433 perspective, it was suggested that a sampling bias could exist, with a better record of temperatures
434 during the warm season at high latitudes and during the cold season in low latitudes (Huber, 2012).
435 Such possible biases would help reduce the model-data discrepancy, in particular for atmospheric

https://doi.org/10.5194/cp-2019-166
Preprint. Discussion started: 14 January 2020


Climate of the Past Discussions
Open Access
EGU

436 temperatures (Fig 10b), as high-latitude reconstructed temperatures are more consistent with
437 simulated summer temperatures whereas the consistency is better with simulated winter
438 temperatures in the mid- to low-latitudes, but more work is required to unambiguously demonstrate
439 the existence of these biases.
440

441 ## 4.2 CRETACEOUS CLIMATE CONTROLLING FACTORS
442

443 The earliest estimates of the temperature change under a doubling of the atmospheric pCO_2
444 predicted a 1.5 to 4.5°C temperature increase, with the most likely scenario at 2.5°C of increase
445 (Barron et al., 1995; IPCC, 2014; Sellers et al., 1996). Our modelling study predicts an atmospheric
446 warming of 11.1°C for the Cretaceous. The signal includes 9°C due to the fourfold increase of pCO_2 or
447 a 4.5°C increase for a doubling of pCO_2 (assuming that the response is linear), which agrees with the
448 high end of the investigations mentioned above. Whilst large, latest generation of earth system
449 models also show an increasingly higher climate sensitivity to increased CO_2 (Golaz et al., 2019;
450 Hutchinson et al., 2018; Niezgodzki et al., 2017), suggesting that the sensitivity could have been
451 underestimated in earlier studies. For example, the recent study of Zhu (2019), using an up-to-date
452 parametrization of cloud microphysics in the CESM1.2 model, proposes an Eocene Climate Sensitivity
453 of 6.6°C for a doubling of CO_2 from 3 to 6 PAL.
454 pCO_2 has been shown here to be the main controlling factor for the atmospheric global
455 warming, whereas the effects of the paleogeography (warming) and reduced solar constant (cooling)
456 nearly cancel each other out (see also Lunt et al., 2016). These results agree with previous studies
457 suggesting that pCO_2 is the main factor controlling the climate (Barron et al., 1995; Crowley and
458 Berner, 2001; Foster et al., 2017; Royer et al., 2007). However, we also demonstrate that the
459 paleogeography plays a major role in the latitudinal distribution of temperatures and impacts oceanic
460 temperatures (with a similar magnitude as a doubling of pCO_2), thus confirming that it is also a critical
461 driver of the Earth's climate (Donnadieu et al., 2006; Fluteau et al., 2007; Lunt et al., 2016; Poulsen et
462 al., 2003). This large effect on climate by the continental configuration has not been reported for
463 paleogeographic configurations more similar to each other, e.g., the Maastrichtian and Cenomanian
464 (Tabor et al., 2016). This is because the main features influencing climate in our study (i.e. the
465 configuration of equatorial and polar zonal connections and the land/sea repartition) do not change a
466 lot between the two geological periods investigated by Tabor et al. (2016). Paleogeography is thus a
467 first-order controller of climate on long scales.
468 It has been suggested that high latitude warming, and an associated reduced meridional SST
469 gradient, was amplified in deep time simulations by rising CO_2 via cloud and vegetation
470 feedbacks (Deconto et al., 2000; Otto-bliesner and Upchurch, 1997) or by increasing ocean heat

https://doi.org/10.5194/cp-2019-166
Preprint. Discussion started: 14 January 2020


Climate of the Past Discussions

transport (Barron et al., 1995; Brady et al., 1998; Schmidt and Mysak, 1996), in particular when changing the paleogeography (Hotinski and Toggweiler, 2003). Our study confirms that the paleogeography is the primary control on the steepness of the oceanic meridional temperature gradient. It is also the only process controlling both the atmosphere and ocean temperature gradients in the tropics. It also has a greater impact than atmospheric CO2 on reducing the atmospheric temperature gradient at high latitudes in the Southern Hemisphere between the Cretaceous and the preindustrial, although the major driver here is the retreat of the polar ice sheets. The increase in pCO_2 appears as the second most important parameter for modifying the SST gradient at high latitudes and it is the main controller of the reduced atmospheric gradient in the North Hemisphere due to low clouds albedo feedback. The effect of paleovegetation on the reduced temperature gradient is not present at high latitudes in our simulations, in contrast to tha warming, up to 4-7°C, reported elsewhere (Deconto et al., 2000; Otto-bliesner and Upchurch, 1997; Upchurch, 1998). Our results thus support the limited influence of vegetation in the Cretaceous high-latitudes warmth (Zhou et al., 2012). However, our modeling setup prescribed boreal vegetation at latitudes higher than 50° ("Boreal broad-leaved summergreen" and "Boreal needleleaf summergreen" PFTs) whereas it was suggested that evergreen forests could possibly develop beyond 60° of latitude (Hay et al., 2019; Sewall et al., 2007) and that temperate forests could extend up to 60° of latitude (Otto-bliesner and Upchurch, 1997). Based on our results, we cannot exclude that this kind of high latitude vegetation can give more weight to the role of paleovegetation in reducing the temperature gradient.

5. CONCLUSIONS

To quantify the impact of major climate forcings on the Cretaceous climate, we performed a series of 6 simulations using the IPSL-CM5A2 earth system model in which we incrementally implement changes in boundary conditions on a pre-industrial simulation to obtain in the end a simulation of the Cenomanian-Turonian stage of the Cretaceous. This study confirms the primary control exerted by atmospheric pCO_2 on atmospheric temperatures, with a contribution of 61% to the total absolute global warming. At the global scale, paleogeographic and solar constant changes have opposite effects, canceling each other, while polar ice cap retreat and vegetation and soil parameter changes have only minor impact. Atmospheric pCO_2 still explains the majority of the global SST warming (49%) but the amount of change explained by paleogeography increases compared to the atmospheric temperature change and thus represents a major contribution (30%). The study of temperature gradients reveals that the reduction of the meridional SST gradients between the preindustrial and the Cretaceous is mainly due to the paleogeographic changes and to a lesser extent to the increase of pCO_2. The atmospheric gradient response is more complex because its flattening is

https://doi.org/10.5194/cp-2019-166
Preprint. Discussion started: 14 January 2020


Climate of the Past Discussions

505 controlled by several factors including paleogeography, pCO2 and polar ice cap retreat, with different
506 answers for the Southern and Northern hemispheres. While predicted oceanic and atmospheric
507 temperatures show a good agreement with data in the low and mid latitudes, predicted temperatures
508 in the high latitudes are colder than paleotemperatures reconstructed from proxies, which leads to
509 steeper equator-to-pole gradients in the model than that calculated from proxies. This mismatch often
510 observed in data-model comparison studies has been reduced in the last decades and could be further
511 resolved by considering possible sampling/seasonal biases in the proxies and by continuously
512 improving the model physics and parameterization. Such modelling efforts would probably even more
513 increase the equilibrium climate sensitivity, which is revised upwards in the latest modelling studies.
514

515 DATA AVAILABILITY

516 Data that support the results of this study are available on request to the authors.

517 AUTHOR CONTRIBUTION

518 M.L performed and analyzed the numerical simulations, in close cooperation with Y.D and J.B.L, and
519 led the writing. M.G run the OTIS model to provide the cenomanian-turonian M2 coefficient. All
520 authors discussed the results and analyses presented in the final version of the manuscript.

521 COMPETING INTERESTS

522 The authors declare that they do not have competing interests.

523 AKNOWLEDGMENTS

524 We express our thanks to Total E&P for funding the project and granting permission to publish. We
525 thank the CEA/CCRT for providing access to the HPC resources of TGCC under the allocation 2018-
526 GEN2212 made by GENCI. J.A.M.G receives funding from the Natural Environmental Research Council
527 (grant NE/S009566/1, MATCH). We acknowledge use of the Ferret (ferret.pmel.noaa.gov/Ferret/)
528 program for analysis and graphics in this paper.

https://doi.org/10.5194/cp-2019-166
Preprint. Discussion started: 14 January 2020

Climate of the Past Discussions
Open Access
EGU

529

530 # FIGURES

531

Figure 1: Time series for oceanic temperatures. (a) Sea-surface temperature and (b) deep-ocean (2500 m) temperature. The piControl and 1X-NOICE simulations are perfectly equilibrated. The 4X simulations still have a small linear drift, around 0.1°C/century or less : 0.07, 0.08, 0.05 and 0.01°C/century during the last 500 yrs for SST of 4X-NOICE, 4X-NOICE-PFT-SOIL, 4X-NOICE-PFT-SOIL-SOLAR and 4X-CRETACEOUS respectively; 0.11, 0.08, 0.07 and 0.06°C/century during the last 500 yrs, for deep-ocean of 4X-NOICE, 4X-NOICE-PFT-SOIL, 4X-NOICE-PFT-SOIL-SOLAR and 4X-CRETACEOUS respectively).

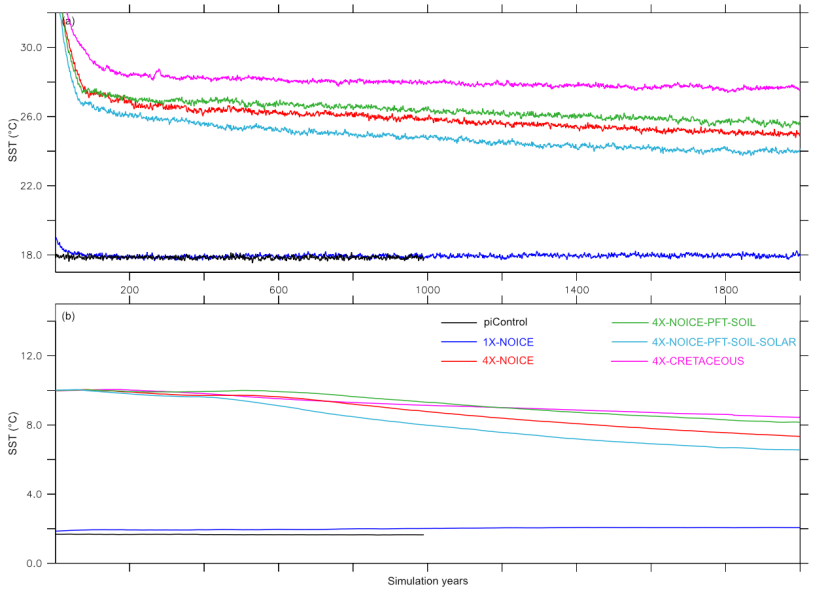

https://doi.org/10.5194/cp-2019-166
Preprint. Discussion started: 14 January 2020

Figure 2: Modern and Cenomanian-Turonian geographic configurations used for the piControl and 4X-CRETACEOUS simulations respectively, and meridional oceanic area anomaly between Cretaceous paleogeography and Modern. geography.

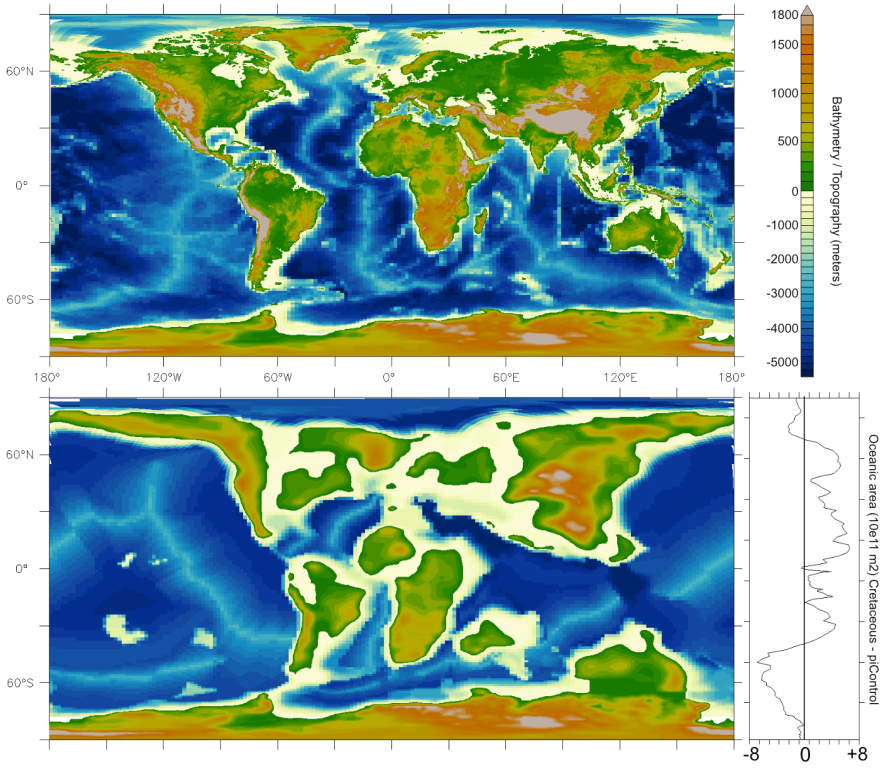

Figure 3: Evolution of Albedo (surface and planetary) and emissivity, in percentages and of T2M (°C) from piControl to 4X-CRETACEOUS simulations. The major change is always recorded with the change of pCO_2 between 1X-NOICE and 4X-NOICE simulations.

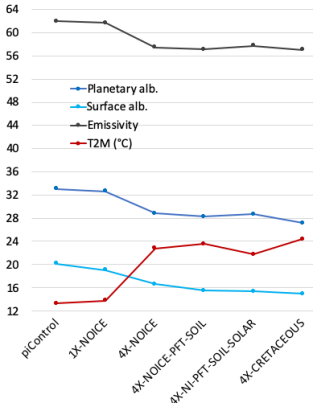

https://doi.org/10.5194/cp-2019-166
Preprint. Discussion started: 14 January 2020

Climate of the Past Discussions
Open Access
EGU

Figure 4: T2M (°C) for (a) piControl initial simulation and (g) Cretaceous final simulation, and anomalies (°C) for intermediate simulations: (b) 1X-NOICE-piControl, (c) 4X-NOICE-1X-NOICE, (d) 4X-NOICE-PFT-SOIL – 4X-NOICE, (e) 4X-NOICE-PFT-SOIL-SOLAR – 4X-NOICE-PFT-SOIL, (f) 4X-CRETACEOUS - 4X-NOICE-PFT-SOIL.

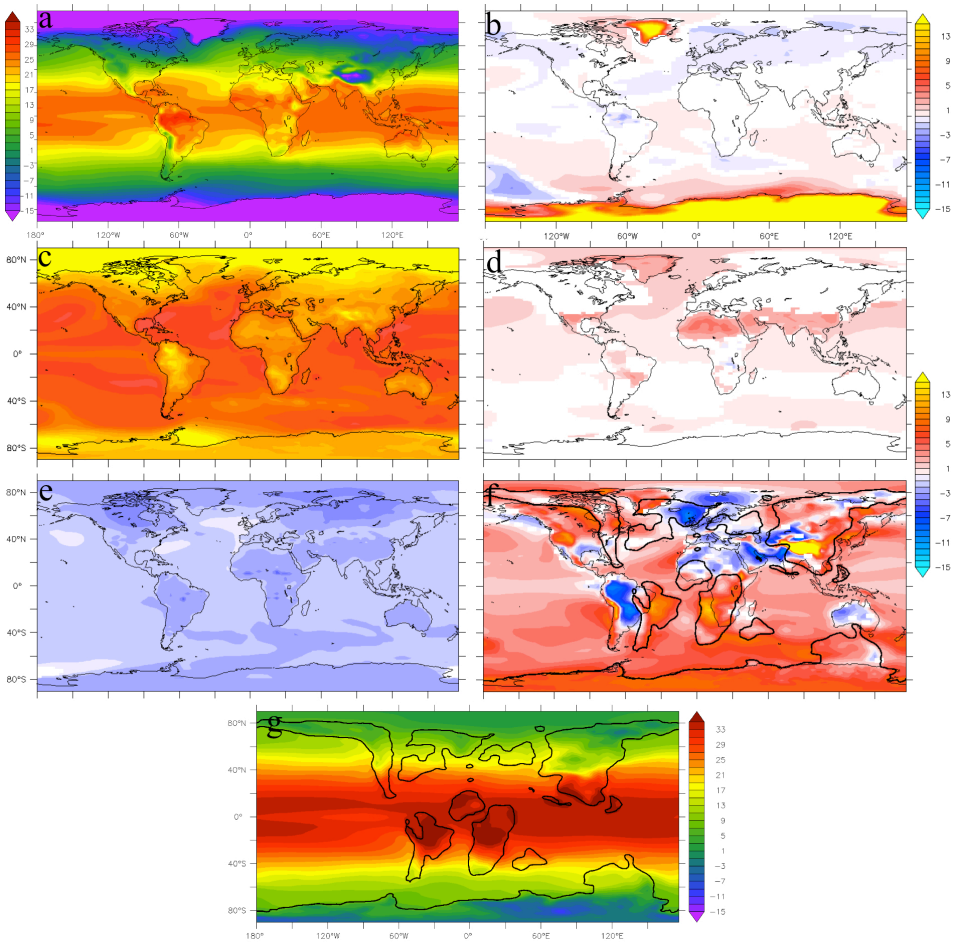

532
533
534
535
536
537
538
539
540
541
542
543

https://doi.org/10.5194/cp-2019-166
Preprint. Discussion started: 14 January 2020

Climate of the Past Discussions
Open Access
EGU

544
545

Figure 5: Cloudiness for 1X-NOICE and 4X-NOICE simulations. (a) Anomaly of total cloudiness (4X-NOICE – 1X NOICE). (b) Low cloudiness (solid curves) and high cloudiness (dashed curves) for 1X-NOICE (black) and 4X-NOICE (red) simulations.

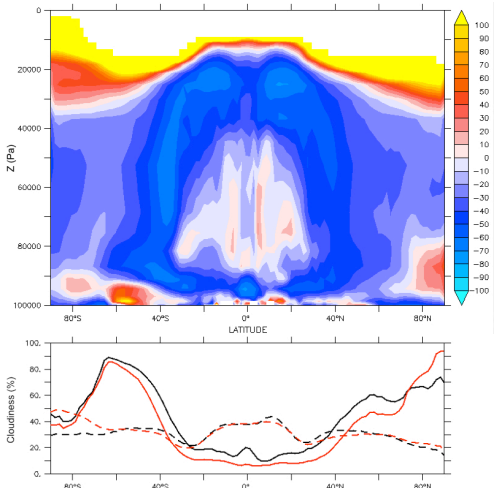

Figure 6: T2M (°C) meridional gradients for 4X-NI-PFT-SOIL-SOLAR-SOLAR (black) and 4X-CRETACEOUS (red) simulations. Solid curve corresponds to annual average, dashed curves correspond to winter and summer values. The 4X-CRETACEOUS simulation is generally warmer than the 4X-NI-PFT-SOIL-SOLAR-SOLAR simulation, with the exception of the boreal summer.

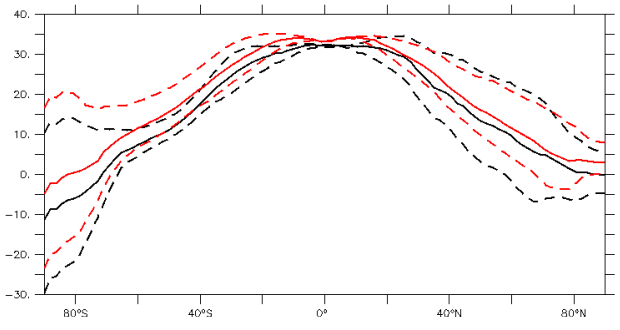

546

https://doi.org/10.5194/cp-2019-166
Preprint. Discussion started: 14 January 2020

Climate of the Past Discussions
Open Access
EGU

Figure 7: Surface currents for 4X-NOICE-PFT-SOIL-SOLAR (left) and 4X-CRETACEOUS (right) simulations. (a), (b) Intensity of surface circulation (Sv – Annual Mean for 0-80 meters of water depth). Strong equatorial winds leads to the formation of an equatorial circumglobal current. (c), (d) Intensity of surface circulation (Sv – Annual Mean for 0-80 meters of water depth). The closure of the Drake passage (DP-300 meters of water depth) leads to the suppression of the ACC.

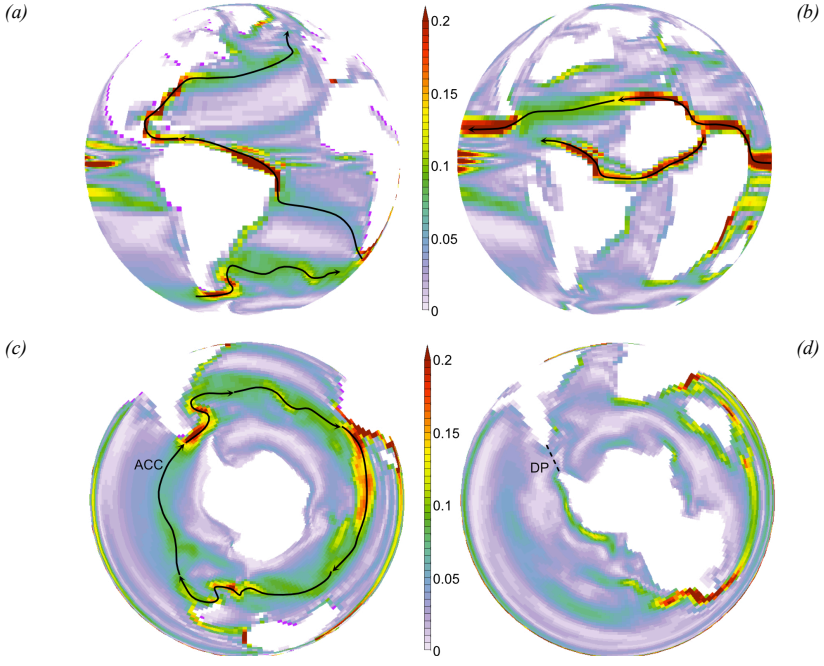

https://doi.org/10.5194/cp-2019-166
Preprint. Discussion started: 14 January 2020

Climate of the Past Discussions

Figure 8 - (a), (b) Global meridional stream-function (sv) for the first 300 meters of water depth. Red and blue colors indicate clockwise and anti-clockwise circulation respectively. (a): 4X-NI-PFT-SOIL-SOLAR and (b) 4X-CRETACEOUS. (c) Oceanic heat transport for 4X-NI-PFT-SOIL-SOLAR and 4X-CRETACEOUS simulations. Positive and negative values indicate northward and southward transport direction, respectively.

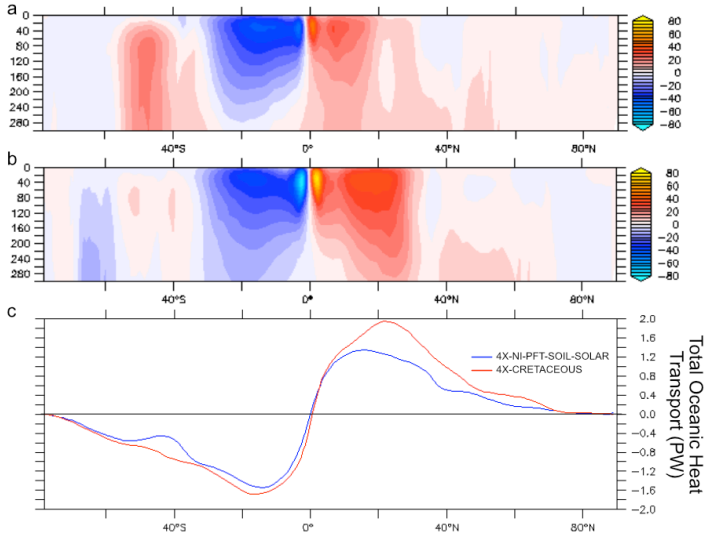

Figure 9: (a) Meridional Sea-Surface Temperature gradients for all simulations. (b) Same SST curves than (a) but superimposed such as equator temperatures are equal, allowing to compare the steepness of the curves. (c) Meridional atmospheric surface temperature gradients for all simulations. (d) Same curves than (c) but superimposed such as equator temperatures are equal.

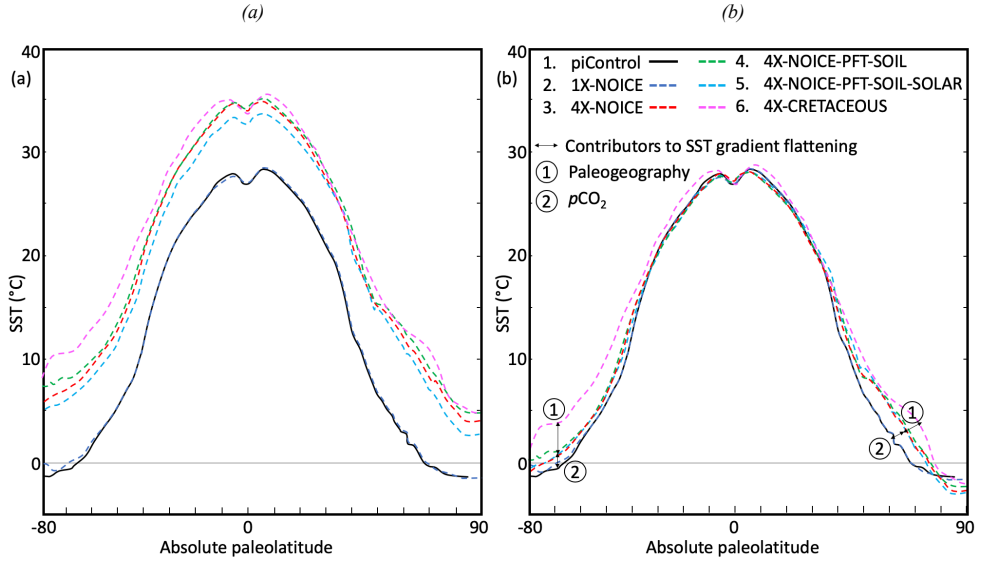

https://doi.org/10.5194/cp-2019-166
Preprint. Discussion started: 14 January 2020

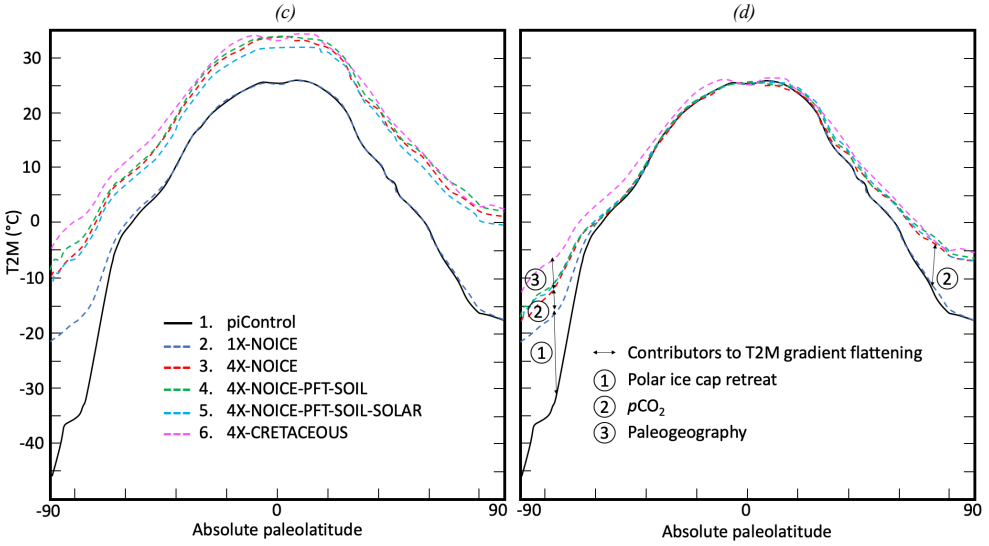

588
589
590
591
592
593
594
595
596
597

598 *Figure 10: Meridional surface temperature gradients for the 4X-CRETACEOUS simulation. (a) Oceanic temperatures: the*
599 *solid line corresponds to the mean annual temperature obtained from the modeling. Dashed lines correspond to winter and*
600 *summer seasonal averages. The grey shaded areas correspond to local monthly temperatures. The red dashed line correspond*
601 *to the regression line calculated from data points. Data points are obtained with several proxies for the cenomano-turonian*
602 *period. The green data point is obtained from TEX 86 for the Maastrichtian (70 Ma) and extrapolated for 90 Ma. The Huber*
603 *et al. (2018) point is obtained from $\delta^{18}0$ on foraminifera and the Vandenmark et al., 2007 point is interpreted from the presence*
604 *of crocodilian fossils. MAT=Mean Annual Temperature, CM=Coldest Month. (b) Atmospheric temperatures: same legend as*
605 *(a) for modelized temperatures. Data points are obtained from several proxies including CLAMP analysis on paleofloras, leaf*
606 *analyses, paleosol-derived climofunction or bioclimatic analysis. Symbols represent mean annual temperatures and solid lines*
607 *associated ranges/errors. Dashed lines represent monthly mean temperatures. Orange data points are for cenomano-turonian*
608 *ages (100-90 Ma), blue data points for Albian and green data points for Coniacian-Santonian (88-85 Ma).*

https://doi.org/10.5194/cp-2019-166
Preprint. Discussion started: 14 January 2020

Climate of the Past
Discussions
Open Access
EGU

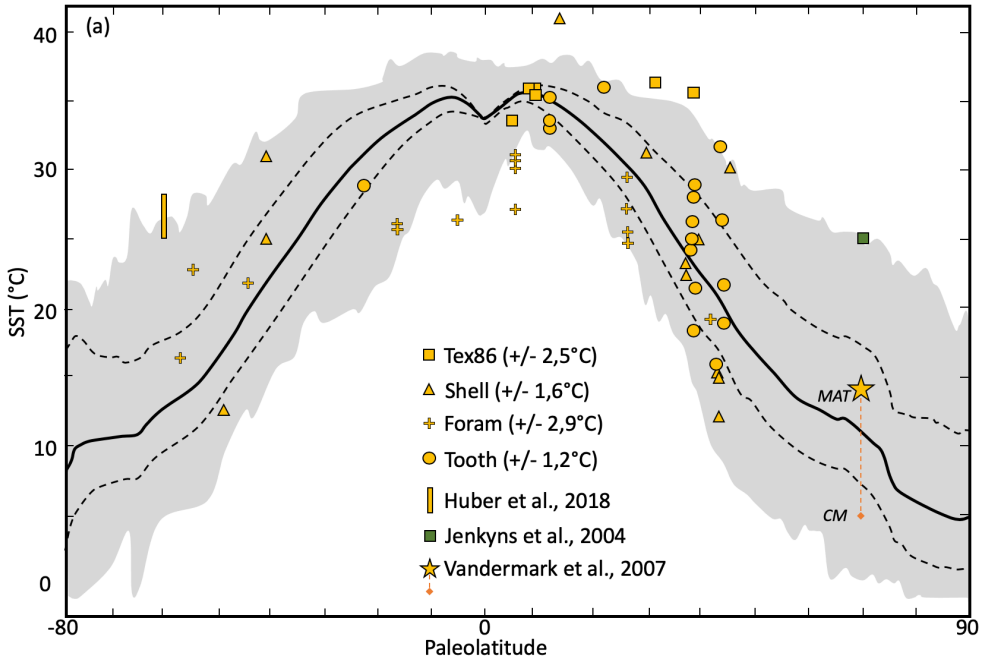

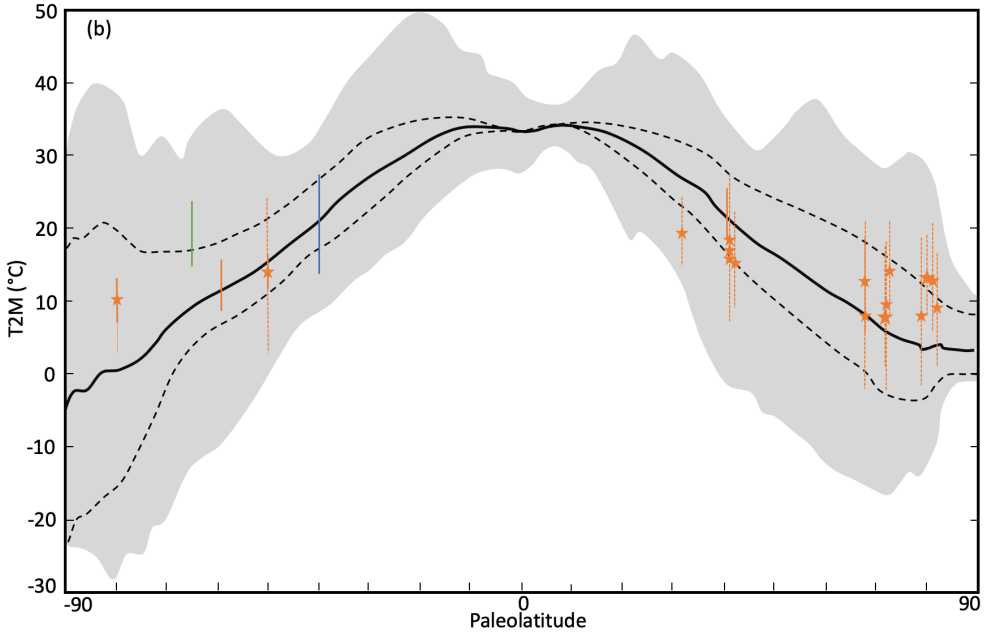

https://doi.org/10.5194/cp-2019-166
Preprint. Discussion started: 14 January 2020

Figure 11: Plot of atmospheric and sea surface temperature gradients vs pCO_2 for different modelling studies and data compilation. Data gradients are plotted for a default pCO_2 value of 4 P.A.L. Gradients are expressed in °C per °latitude and are calculated from 30 to 80 degrees of latitude.

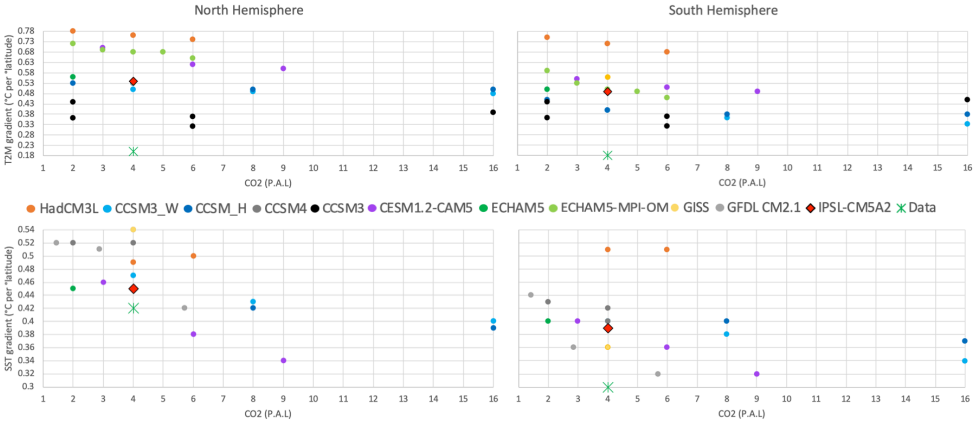

REFERENCES

Aumont, O. and Bopp, L.: Globalizing results from ocean in situ iron fertilization studies, Global Biogeochem. Cycles, 20(2), 1–15, doi:10.1029/2005GB002591, 2006.

Aumont, O., Ethé, C., Tagliabue, A., Bopp, L. and Gehlen, M.: PISCES-v2: An ocean biogeochemical model for carbon and ecosystem studies, Geosci. Model Dev., 8(8), 2465–2513, doi:10.5194/gmd-8-2465-2015, 2015.

Barclay, R. S., McElwain, J. C. and Sageman, B. B.: Carbon sequestration activated by a volcanic CO 2 pulse during Ocean Anoxic Event 2, Nat. Geosci., 3(3), 205–208, doi:10.1038/ngeo757, 2010.

Barron, E. J.: Model simulations of Cretaceous climates : the role of geography and carbon dioxide, , 1(1989), 1993.

Barron, E. J., Fawcett, P. J., Peterson, W. H., Pollard, D. and Thompson, S. L.: A " simulation " of mid-Cretaceous climate Abstract . A series of general circulation model experiments W increased from present day). By combining all three major variables levels of CO2 . Four times present-day • s W provided the best match to the this, , 10(5), 953–962, 1995.

https://doi.org/10.5194/cp-2019-166
Preprint. Discussion started: 14 January 2020

631 Van Bentum, E. C., Reichart, G. J., Forster, A. and Sinninghe Damsté, J. S.: Latitudinal
632 differences in the amplitude of the OAE-2 carbon isotopic excursion: PCO2and paleo
633 productivity, Biogeosciences, 9(2), 717–731, doi:10.5194/bg-9-717-2012, 2012.
634 Berner, R. A.: GEOCARBSULF: A combined model for Phanerozoic atmospheric O2 and
635 CO2, Geochim. Cosmochim. Acta, 70(23 SPEC. ISS.), 5653–5664,
636 doi:10.1016/j.gca.2005.11.032, 2006.
637 Bice, K. L. and Norris, R. D.: Possible atmospheric CO 2 extremes of the Middle Cretaceous
638 (late Albian-Turonian) , Paleoceanography, 17(4), 22-1-22–17, doi:10.1029/2002pa000778,
639 2003.
640 Bice, K. L., Birgel, D., Meyers, P. A., Dahl, K. A., Hinrichs, K. U. and Norris, R. D.: A
641 multiple proxy and model study of Cretaceous upper ocean temperatures and atmospheric
642 CO2 concentrations, Paleoceanography, 21(2), 1–17, doi:10.1029/2005PA001203, 2006.
643 Bopp, L., Resplandy, L., Orr, J. C., Doney, S. C., Dunne, J. P., Gehlen, M., Halloran, P.,
644 Heinze, C., Ilyina, T., Séférian, R., Tjiputra, J. and Vichi, M.: Multiple stressors of ocean
645 ecosystems in the 21st century: Projections with CMIP5 models, Biogeosciences, 10(10),
646 6225–6245, doi:10.5194/bg-10-6225-2013, 2013.
647 Bopp, L., Resplandy, L., Untersee, A., Le Mezo, P. and Kageyama, M.: Ocean
648 (de)oxygenation from the Last Glacial Maximum to the twenty-first century: Insights from
649 Earth System models, Philos. Trans. R. Soc. A Math. Phys. Eng. Sci., 375(2102),
650 doi:10.1098/rsta.2016.0323, 2017.
651 Brady, E. C., Deconto, R. M. and Thompson, S. L.: Deep Water Formation and Poleward
652 Ocean Heat Transport in the Warm Climate Extreme of the Cretaceous (80 Ma) evidence, ,
653 25(22), 4205–4208, 1998.
654 Broccoli, A. J. and Manabe, S.: The influence of continental ice, atmospheric CO2, and land
655 albedo on the climate of the last glacial maximum, Clim. Dyn., 1(2), 87–99,
656 doi:10.1007/BF01054478, 1987.
657 Bush, A. B. G., George, S. and Philander, H.: The late Cretaceous ' Simulation with a coupled
658 atmosphere-ocean general circulation model, , 12(3), 495–516, 1997.
659 Contoux, C., Jost, A., Ramstein, G., Sepulchre, P., Krinner, G. and Schuster, M.: Megalake
660 chad impact on climate and vegetation during the late Pliocene and the mid-Holocene, Clim.
661 Past, 9(4), 1417–1430, doi:10.5194/cp-9-1417-2013, 2013.
662 Contoux, C., Dumas, C., Ramstein, G., Jost, A. and Dolan, A. M.: Modelling Greenland ice
663 sheet inception and sustainability during the Late Pliocene, Earth Planet. Sci. Lett., 424, 295–
664 305, doi:10.1016/j.epsl.2015.05.018, 2015.

https://doi.org/10.5194/cp-2019-166
Preprint. Discussion started: 14 January 2020

665 Crowley, T. J. and Berner, R. A.: CO2 and climate change, Science (80-.)., 292(5518), 870–
666 872, doi:10.1126/science.1061664, 2001.
667 Crowley, T. J. and Zachos, J. C.: Comparison of zonal temperature profiles for past warm
668 time periods, in Warm Climates in Earth History, edited by B. T. Huber, K. G. Macleod, and
669 S. L. Wing, pp. 50–76, Cambridge University Press, Cambridge., 1999.
670 Crowley, T. J., Short, D. A., Mengel, J. G. and North, G. R.: Role of seasonality in the
671 evolution of climate during the last 100 million years, Science (80-.)., 231(4738), 579–584,
672 doi:10.1126/science.231.4738.579, 1986.
673 Damsté, J. S. S., Kuypers, M. M. M., Pancost, R. D. and Schouten, S.: The carbon isotopic
674 response of algae, (cyano)bacteria, archaea and higher plants to the late Cenomanian
675 perturbation of the global carbon cycle: Insights from biomarkers in black shales from the
676 Cape Verde Basin (DSDP Site 367), Org. Geochem., 39(12), 1703–1718,
677 doi:10.1016/j.orggeochem.2008.01.012, 2008.
678 Deconto, R. M., Brady, E. C., Bergengren, J. and Hay, W. W.: Late Cretaceous climate,
679 vegetation, and ocean interactions, Warm Clim. Earth Hist., 275–296,
680 doi:10.1017/cbo9780511564512.010, 2000.
681 Von Deimling, T. S., Ganopolski, A., Held, H. and Rahmstorf, S.: How cold was the last
682 Glacial maximum?, Geophys. Res. Lett., 33(14), 1–5, doi:10.1029/2006GL026484, 2006.
683 Donnadieu, Y., Pierrehumbert, R., Jacob, R. and Fluteau, F.: Modelling the primary control of
684 paleogeography on Cretaceous climate, Earth Planet. Sci. Lett., 248(1–2), 411–422,
685 doi:10.1016/j.epsl.2006.06.007, 2006.
686 Dufresne, J. L., Foujols, M. A., Denvil, S., Caubel, A., Marti, O., Aumont, O., Balkanski, Y.,
687 Bekki, S., Bellenger, H., Benshila, R., Bony, S., Bopp, L., Braconnot, P., Brockmann, P.,
688 Cadule, P., Cheruy, F., Codron, F., Cozic, A., Cugnet, D., de Noblet, N., Duvel, J. P., Ethé,
689 C., Fairhead, L., Fichefet, T., Flavoni, S., Friedlingstein, P., Grandpeix, J. Y., Guez, L.,
690 Guilyardi, E., Hauglustaine, D., Hourdin, F., Idelkadi, A., Ghattas, J., Joussaume, S.,
691 Kageyama, M., Krinner, G., Labetoulle, S., Lahellec, A., Lefebvre, M. P., Lefevre, F., Levy,
692 C., Li, Z. X., Lloyd, J., Lott, F., Madec, G., Mancip, M., Marchand, M., Masson, S.,
693 Meurdesoif, Y., Mignot, J., Musat, I., Parouty, S., Polcher, J., Rio, C., Schulz, M.,
694 Swingedouw, D., Szopa, S., Talandier, C., Terray, P., Viovy, N. and Vuichard, N.: Climate
695 change projections using the IPSL-CM5 Earth System Model: From CMIP3 to CMIP5., 2013.
696 Egbert, G. D., Ray, R. D. and Bills, B. G.: Numerical modeling of the global semidiurnal tide
697 in the present day and in the last glacial maximum, J. Geophys. Res. C Ocean., 109(3), 1–15,
698 doi:10.1029/2003jc001973, 2004.

https://doi.org/10.5194/cp-2019-166
Preprint. Discussion started: 14 January 2020

699 Enderton, D. and Marshall, J.: Explorations of Atmosphere–Ocean–Ice Climates on an
700 Aquaplanet and Their Meridional Energy Transports, J. Atmos. Sci., 66(6), 1593–1611,
701 doi:10.1175/2008jas2680.1, 2008.
702 Fichefet, T. and Maqueda, M. A. M.: Sensitivity of a global sea ice model to the treatment of
703 ice thermodynamics and dynamics, J. Geophys. Res. Ocean., 102(C6), 12609–12646,
704 doi:10.1029/97JC00480, 1997.
705 Fletcher, B. J., Brentnall, S. J., Quick, W. P. and Beerling, D. J.: BRYOCARB: A process-
706 based model of thallose liverwort carbon isotope fractionation in response to CO2, O2, light
707 and temperature, Geochim. Cosmochim. Acta, 70(23 SPEC. ISS.), 5676–5691,
708 doi:10.1016/j.gca.2006.01.031, 2006.
709 Fluteau, F., Ramstein, G., Besse, J., Guiraud, R. and Masse, J. P.: Impacts of palaeogeography
710 and sea level changes on Mid-Cretaceous climate, Palaeogeogr. Palaeoclimatol. Palaeoecol.,
711 247(3–4), 357–381, doi:10.1016/j.palaeo.2006.11.016, 2007.
712 Foster, G. L., Royer, D. L. and Lunt, D. J.: Future climate forcing potentially without
713 precedent in the last 420 million years, Nat. Commun., 8, 1–8, doi:10.1038/ncomms14845,
714 2017.
715 Friedrich, O., Norris, R. D. and Erbacher, J.: Evolution of middle to late Cretaceous oceans-A
716 55 m.y. Record of Earth's temperature and carbon cycle, Geology, 40(2), 107–110,
717 doi:10.1130/G32701.1, 2012.
718 Gastineau, G., D'Andrea, F. and Frankignoul, C.: Atmospheric response to the North Atlantic
719 Ocean variability on seasonal to decadal time scales, Clim. Dyn., 40(9–10), 2311–2330,
720 doi:10.1007/s00382-012-1333-0, 2013.
721 Gates, W. L., Boyle, J. S., Covey, C., Dease, C. G., Doutriaux, C. M., Drach, R. S., Fiorino,
722 M., Gleckler, P. J., Hnilo, J. J., Marlais, S. M., Phillips, T. J., Potter, G. L., Santer, B. D.,
723 Sperber, K. R., Taylor, K. E. and Williams, D. N.: An Overview of the Results of the
724 Atmospheric Model Intercomparison Project (AMIP I), Bull. Am. Meteorol. Soc., 80(1), 29–
725 55 [online] Available from: http://www.jstor.org/stable/26214897, 1999.
726 Goddéris, Y., Donnadieu, Y., Le Hir, G., Lefebvre, V. and Nardin, E.: The role of
727 palaeogeography in the Phanerozoic history of atmospheric CO2and climate, Earth-Science
728 Rev., 128, 122–138, doi:10.1016/j.earscirev.2013.11.004, 2014.
729 Golaz, J., Caldwell, P. M., Van Roekel, L. P., Petersen, M. R., Tang, Q., Wolfe, J. D.,
730 Abeshu, G., Anantharaj, V., Asay-Davis, X. S., Bader, D. C., Baldwin, S. A., Bisht, G.,
731 Bogenschutz, P. A., Branstetter, M., Brunke, M. A., Brus, S. R., Burrows, S. M., Cameron-
732 Smith, P. J., Donahue, A. S., Deakin, M., Easter, R. C., Evans, K. J., Feng, Y., Flanner, M.,

https://doi.org/10.5194/cp-2019-166
Preprint. Discussion started: 14 January 2020

733 Foucar, J. G., Fyke, J. G., Griffin, B. M., Hannay, C., Harrop, B. E., Hunke, E. C., Jacob, R.
734 L., Jacobsen, D. W., Jeffery, N., Jones, P. W., Keen, N. D., Klein, S. A., Larson, V. E.,
735 Leung, L. R., Li, H., Lin, W., Lipscomb, W. H., Ma, P., Mahajan, S., Maltrud, M. E.,
736 Mametjanov, A., McClean, J. L., McCoy, R. B., Neale, R. B., Price, S. F., Qian, Y., Rasch, P.
737 J., Reeves Eyre, J. E. J., Riley, W. J., Ringler, T. D., Roberts, A. F., Roesler, E. L., Salinger,
738 A. G., Shaheen, Z., Shi, X., Singh, B., Tang, J., Taylor, M. A., Thornton, P. E., Turner, A. K.,
739 Veneziani, M., Wan, H., Wang, H., Wang, S., Williams, D. N., Wolfram, P. J., Worley, P. H.,
740 Xie, S., Yang, Y., Yoon, J., Zelinka, M. D., Zender, C. S., Zeng, X., Zhang, C., Zhang, K.,
741 Zhang, Y., Zheng, X., Zhou, T. and Zhu, Q.: The DOE E3SM coupled model version 1:
742 Overview and evaluation at standard resolution, J. Adv. Model. Earth Syst., 1–82,
743 doi:10.1029/2018ms001603, 2019.
744 Goldner, A., Herold, N. and Huber, M.: Antarctic glaciation caused ocean circulation changes
745 at the Eocene-Oligocene transition, Nature, 511(7511), 574–577, doi:10.1038/nature13597,
746 2014.
747 Gough: Solar interior structure variations*, Sol. Phys., 74(September 1980), 21–34, 1981.
748 Green, J. A. M. and Huber, M.: Tidal dissipation in the early Eocene and implications for
749 ocean mixing, Geophys. Res. Lett., 40(11), 2707–2713, doi:10.1002/grl.50510, 2013.
750 Gyllenhaal, E. D., Engberts, C. J., Markwick, P. J., Smith, L. H. and Patzkowsky, M. E.: The
751 Fujita-Ziegler model: a new semi-quantitative technique for estimating paleoclimate from
752 paleogeographic maps, Palaeogeogr. Palaeoclimatol. Palaeoecol., 86(1–2), 41–66,
753 doi:10.1016/0031-0182(91)90005-C, 1991.
754 Hay, W. W., DeConto, R. M., de Boer, P., Flögel, S., Song, Y. and Stepashko, A.: Possible
755 solutions to several enigmas of Cretaceous climate, Springer Berlin Heidelberg., 2019.
756 Heinemann, M., Jungclaus, J. H. and Marotzke, J.: Warm Paleocene/Eocene climate as
757 simulated in ECHAM5/MPI-OM, Clim. Past, 5(4), 785–802, doi:10.5194/cp-5-785-2009,
758 2009.
759 Herman, A. B. and Spicer, R. A.: Palaeobotanical evidence for a warm Cretaceous Arctic
760 Ocean, Nature, 380(6572), 330–333, doi:10.1038/380330a0, 1996.
761 Herman, A. B. and Spicer, R. A.: Mid-Cretaceous floras and climate of the Russian high
762 Arctic (Novosibirsk Islands, Northern Yakutiya), Palaeogeogr. Palaeoclimatol. Palaeoecol.,
763 295(3–4), 409–422, doi:10.1016/j.palaeo.2010.02.034, 2010.
764 Herweijer, C., Seager, R., Winton, M. and Clement, A.: Why ocean heat transport warms the
765 global mean climate, Tellus, Ser. A Dyn. Meteorol. Oceanogr., 57(4), 662–675,
766 doi:10.1111/j.1600-0870.2005.00121.x, 2005.

https://doi.org/10.5194/cp-2019-166
Preprint. Discussion started: 14 January 2020

767 Hong, S. K. and Lee, Y. Il: Evaluation of atmospheric carbon dioxide concentrations during
768 the Cretaceous, Earth Planet. Sci. Lett., 327–328, 23–28, doi:10.1016/j.epsl.2012.01.014,
769 2012.
770 Hotinski, R. M. and Toggweiler, J. R.: Impact of a Tethyan circumglobal passage on ocean
771 heat transport and "equable" climates, Paleoceanography, 18(1), n/a-n/a,
772 doi:10.1029/2001PA000730, 2003.
773 Hourdin, F., Foujols, M. A., Codron, F., Guemas, V., Dufresne, J. L., Bony, S., Denvil, S.,
774 Guez, L., Lott, F., Ghattas, J., Braconnot, P., Marti, O., Meurdesoif, Y. and Bopp, L.: Impact
775 of the LMDZ atmospheric grid configuration on the climate and sensitivity of the IPSL-
776 CM5A coupled model, Clim. Dyn., 40(9–10), 2167–2192, doi:10.1007/s00382-012-1411-3,
777 2013.
778 Huber, B. T., Hodell, D. A. and Hamilton, C. P.: … Late Cretaceous climate of the southern
779 high latitudes: Stable isotopic evidence for minimal …, Geol. Soc. Am. Bull., (10), 1164–
780 1191, doi:10.1130/0016-7606(1995)107<1164, 1995.
781 Huber, B. T., Leckie, R. M., Norris, R. D., Bralower, T. J. and CoBabe, E.: Foraminiferal
782 assemblage and stable isotopic change across the Cenomanian-Turonian boundary in the
783 Subtropical North Atlantic, J. Foraminifer. Res., 29(4), 392–417, 1999.
784 Huber, B. T., Norris, R. D. and MacLeod, K. G.: Deep-sea paleotemperature record of
785 extreme warmth during the Cretaceous, Geology, 30(2), 123–126, doi:10.1130/0091-
786 7613(2002)030<0123:DSPROE>2.0.CO;2, 2002.
787 Huber, B. T., MacLeod, K. G., Watkins, D. K. and Coffin, M. F.: The rise and fall of the
788 Cretaceous Hot Greenhouse climate, Glob. Planet. Change, 167(April), 1–23,
789 doi:10.1016/j.gloplacha.2018.04.004, 2018.
790 Huber, M.: Progress in Greenhouse Climate Modeling, Paleontol. Soc. Pap., 18, 213–262,
791 doi:10.1017/s108933260000262x, 2012.
792 Huber, M. and Caballero, R.: The early Eocene equable climate problem revisited, Clim. Past,
793 7(2), 603–633, doi:10.5194/cp-7-603-2011, 2011.
794 Hunter, S. J., Haywood, A. M., Valdes, P. J., Francis, J. E. and Pound, M. J.: Modelling
795 equable climates of the Late Cretaceous: Can new boundary conditions resolve data-model
796 discrepancies?, Palaeogeogr. Palaeoclimatol. Palaeoecol., 392, 41–51,
797 doi:10.1016/j.palaeo.2013.08.009, 2013.
798 Hutchinson, D. K., De Boer, A. M., Coxall, H. K., Caballero, R., Nilsson, J. and Baatsen, M.:
799 Climate sensitivity and meridional overturning circulation in the late Eocene using GFDL
800 CM2.1, Clim. Past, 14(6), 789–810, doi:10.5194/cp-14-789-2018, 2018.

https://doi.org/10.5194/cp-2019-166
Preprint. Discussion started: 14 January 2020

801 IPCC: Climate Change 2014: Synthesis Report. Contribution of Working Groups I, II and III
802 to the Fifth Assessment Report of the Intergovernmental Panel on Climate Change., 2014.
803 Jenkyns, H. C.: Geochemistry of oceanic anoxic events, Geochemistry, Geophys.
804 Geosystems, 11(3), 1–30, doi:10.1029/2009GC002788, 2010.
805 Jenkyns, H. C., Forster, A., Schouten, S. and Sinninghe Damsté, J. S.: High temperatures in
806 the Late Cretaceous Arctic Ocean, Nature, 432(7019), 888–892, doi:10.1038/nature03143,
807 2004.
808 Kageyama, M., Braconnot, P., Bopp, L., Caubel, A., Foujols, M. A., Guilyardi, E., Khodri,
809 M., Lloyd, J., Lombard, F., Mariotti, V., Marti, O., Roy, T. and Woillez, M. N.: Mid-
810 Holocene and Last Glacial Maximum climate simulations with the IPSL model-part I:
811 Comparing IPSL_CM5A to IPSL_CM4, Clim. Dyn., 40(9–10), 2447–2468,
812 doi:10.1007/s00382-012-1488-8, 2013.
813 Kennedy, A. T., Farnsworth, A., Lunt, D. J., Lear, C. H. and Markwick, P. J.: Atmospheric
814 and oceanic impacts of Antarctic glaciation across the Eocene-Oligocene transition, Philos.
815 Trans. R. Soc. A Math. Phys. Eng. Sci., 373(2054), doi:10.1098/rsta.2014.0419, 2015.
816 Kerr, A. C. and Kerr, A. C.: Oceanic plateau formation : A cause of mass extinction and black
817 shale deposition around the Cenomanian-Turonian boundary ? Oceanic plateau formation : a
818 cause of mass extinction and black shale deposition around the Cenomanian – Turonian
819 boundary ?, , (May), doi:10.1144/gsjgs.155.4.0619, 1998.
820 Knorr, G. and Lohmann, G.: Climate warming during antarctic ice sheet expansion at the
821 middle miocene transition, Nat. Geosci., 7(5), 376–381, doi:10.1038/ngeo2119, 2014.
822 Koch-Larrouy, A., Madec, G., Bouruet-Aubertot, P., Gerkema, T., Bessières, L. and Molcard,
823 R.: On the transformation of Pacific Water into Indonesian Throughflow Water by internal
824 tidal mixing, Geophys. Res. Lett., 34(4), 1–6, doi:10.1029/2006GL028405, 2007.
825 Krinner, G., Viovy, N., de Noblet-Ducoudré, N., Ogée, J., Polcher, J., Friedlingstein, P.,
826 Ciais, P., Sitch, S. and Prentice, I. C.: A dynamic global vegetation model for studies of the
827 coupled atmosphere-biosphere system, Global Biogeochem. Cycles, 19(1), 1–33,
828 doi:10.1029/2003GB002199, 2005.
829 Ladant, J. B. and Donnadieu, Y.: Palaeogeographic regulation of glacial events during the
830 Cretaceous supergreenhouse, Nat. Commun., 7(April 2017), 1–9, doi:10.1038/ncomms12771,
831 2016.
832 Ladant, J. B., Donnadieu, Y., Bopp, L., Lear, C. H. and Wilson, P. A.: Meridional Contrasts
833 in Productivity Changes Driven by the Opening of Drake Passage, Paleoceanogr.
834 Paleoclimatology, 302–317, doi:10.1002/2017PA003211, 2018.

https://doi.org/10.5194/cp-2019-166
Preprint. Discussion started: 14 January 2020

de Lavergne, C., Falahat, S., Madec, G., Roquet, F., Nycander, J. and Vic, C.: Toward global maps of internal tide energy sinks, Ocean Model., 137(April), 52–75, doi:10.1016/j.ocemod.2019.03.010, 2019.

Leier, A., Quade, J., DeCelles, P. and Kapp, P.: Stable isotopic results from paleosol carbonate in South Asia: Paleoenvironmental reconstructions and selective alteration, Earth Planet. Sci. Lett., 279(3–4), 242–254, doi:10.1016/j.epsl.2008.12.044, 2009.

Levine, X. J. and Schneider, T.: Response of the Hadley Circulation to Climate Change in an Aquaplanet GCM Coupled to a Simple Representation of Ocean Heat Transport, J. Atmos. Sci., 68(4), 769–783, doi:10.1175/2010jas3553.1, 2010.

Littler, K., Robinson, S. A., Bown, P. R., Nederbragt, A. J. and Pancost, R. D.: High sea-surface temperatures during the Early Cretaceous Epoch, Nat. Geosci., 4(3), 169–172, doi:10.1038/ngeo1081, 2011.

Lunt, D. J., Jones, T. D., Heinemann, M., Huber, M., LeGrande, A., Winguth, A., Loptson, C., Marotzke, J., Roberts, C. D., Tindall, J., Valdes, P. and Winguth, C.: A model-data comparison for a multi-model ensemble of early Eocene atmosphere-ocean simulations: EoMIP, Clim. Past, 8(5), 1717–1736, doi:10.5194/cp-8-1717-2012, 2012a.

Lunt, D. J., Haywood, A. M., Schmidt, G. A., Salzmann, U., Valdes, P. J., Dowsett, H. J. and Loptson, C. A.: On the causes of mid-Pliocene warmth and polar amplification, Earth Planet. Sci. Lett., 321–322, 128–138, doi:10.1016/j.epsl.2011.12.042, 2012b.

Lunt, D. J., Farnsworth, A., Loptson, C., L Foster, G., Markwick, P., O'Brien, C. L., Pancost, R. D., Robinson, S. A. and Wrobel, N.: Palaeogeographic controls on climate and proxy interpretation, Clim. Past, 12(5), 1181–1198, doi:10.5194/cp-12-1181-2016, 2016.

Lunt, D. J., Huber, M., Anagnostou, E., Baatsen, M. L. J., Caballero, R., DeConto, R., Dijkstra, H. A., Donnadieu, Y., Evans, D., Feng, R., Foster, G. L., Gasson, E., Von Der Heydt, A. S., Hollis, C. J., Inglis, G. N., Jones, S. M., Kiehl, J., Turner, S. K., Korty, R. L., Kozdon, R., Krishnan, S., Ladant, J. B., Langebroek, P., Lear, C. H., LeGrande, A. N., Littler, K., Markwick, P., Otto-Bliesner, B., Pearson, P., Poulsen, C. J., Salzmann, U., Shields, C., Snell, K., Stärz, M., Super, J., Tabor, C., Tierney, J. E., Tourte, G. J. L., Tripati, A., Upchurch, G. R., Wade, B. S., Wing, S. L., Winguth, A. M. E., Wright, N. M., Zachos, J. C. and Zeebe, R. E.: The DeepMIP contribution to PMIP4: Experimental design for model simulations of the EECO, PETM, and pre-PETM (version 1.0), Geosci. Model Dev., 10(2), 889–901, doi:10.5194/gmd-10-889-2017, 2017.

MacLeod, K. G., Huber, B. T., Berrocoso, Á. J. and Wendler, I.: A stable and hot Turonian without glacial δ18O excursions is indicated by exquisitely preserved Tanzanian foraminifera,

https://doi.org/10.5194/cp-2019-166
Preprint. Discussion started: 14 January 2020

Geology, 41(10), 1083–1086, doi:10.1130/G34510.1, 2013.

Madec, G.: NEMO ocean engine (2012), , (27), 2012.

Madec, G. and Imbard, M.: A global ocean mesh to overcome the North Pole singularity, Clim. Dyn., 12(6), 381–388, doi:10.1007/BF00211684, 1996.

Maffre, P., Ladant, J. B., Donnadieu, Y., Sepulchre, P. and Goddéris, Y.: The influence of orography on modern ocean circulation, Clim. Dyn., 50(3–4), 1277–1289, doi:10.1007/s00382-017-3683-0, 2018.

Mays, C., Steinthorsdottir, M. and Stilwell, J. D.: Climatic implications of Ginkgoites waarrensis Douglas emend. from the south polar Tupuangi flora, Late Cretaceous (Cenomanian), Chatham Islands, Palaeogeogr. Palaeoclimatol. Palaeoecol., 438, 308–326, doi:10.1016/j.palaeo.2015.08.011, 2015.

Le Mézo, P., Beaufort, L., Bopp, L., Braconnot, P. and Kageyama, M.: From monsoon to marine productivity in the Arabian Sea: Insights from glacial and interglacial climates, Clim. Past, 13(7), 759–778, doi:10.5194/cp-13-759-2017, 2017.

Monteiro, F. M., Pancost, R. D., Ridgwell, A. and Donnadieu, Y.: Nutrients as the dominant control on the spread of anoxia and euxinia across the Cenomanian-Turonian oceanic anoxic event (OAE2): Model-data comparison, Paleoceanography, 27(4), 1–17, doi:10.1029/2012PA002351, 2012.

Müller, R. D., Sdrolias, M., Gaina, C. and Roest, W. R.: Age, spreading rates, and spreading asymmetry of the world's ocean crust, Geochemistry, Geophys. Geosystems, 9(4), 1–19, doi:10.1029/2007GC001743, 2008.

Niezgodzki, I., Knorr, G., Lohmann, G., Tyszka, J. and Markwick, P. J.: Late Cretaceous climate simulations with different CO2 levels and subarctic gateway configurations: A model-data comparison, Paleoceanography, 32(9), 980–998, doi:10.1002/2016PA003055, 2017.

Norris, R. D., Bice, K. L., Magno, E. A. and Wilson, P. A.: Jiggling the tropical thermostat in the Cretaceous hothouse, Geology, 30(4), 299–302, doi:10.1130/0091-7613(2002)030<0299:JTTTIT>2.0.CO;2, 2002.

O'Brien, C. L., Robinson, S. A., Pancost, R. D., Sinninghe Damsté, J. S., Schouten, S., Lunt, D. J., Alsenz, H., Bornemann, A., Bottini, C., Brassell, S. C., Farnsworth, A., Forster, A., Huber, B. T., Inglis, G. N., Jenkyns, H. C., Linnert, C., Littler, K., Markwick, P., McAnena, A., Mutterlose, J., Naafs, B. D. A., Püttmann, W., Sluijs, A., van Helmond, N. A. G. M., Vellekoop, J., Wagner, T. and Wrobel, N. E.: Cretaceous sea-surface temperature evolution: Constraints from TEX 86 and planktonic foraminiferal oxygen isotopes, Earth-Science Rev., 172(March 2016), 224–247, doi:10.1016/j.earscirev.2017.07.012, 2017.

https://doi.org/10.5194/cp-2019-166
Preprint. Discussion started: 14 January 2020

903 Ohba, M. and Ueda, H.: A GCM Study on Effects of Continental Drift on Tropical Climate at
904 the Early and Late Cretaceous, J. Meteorol. Soc. Japan, 88(6), 869–881,
905 doi:10.2151/jmsj.2010-601, 2011.
906 Ortega, P., Mignot, J., Swingedouw, D., Sévellec, F. and Guilyardi, E.: Reconciling two
907 alternative mechanisms behind bi-decadal variability in the North Atlantic, Prog. Oceanogr.,
908 137, 237–249, doi:10.1016/j.pocean.2015.06.009, 2015.
909 Otto-bliesner, B. L. and Upchurch, G. R.: the Late Cretaceous period, , 385127(February),
910 18–21, 1997.
911 Pearson, P. N., DitchfieldPeter, W., SinganoJoyce, Harcourt-BrownKatherine, G.,
912 NicholasChristopher, J., OlssonRichard, K., ShackletonNicholas, J. and HallMike, A.:
913 erratum: Warm tropical sea surface temperatures in the Late Cretaceous and Eocene epochs,
914 Nature, 414(6862), 470 [online] Available from: http://dx.doi.org/10.1038/35106617, 2001.
915 Poulsen, C. J., Seidov, D., Barron, E. J. and Peterson, W. H.: The impact of paleogeographic
916 evolution on the surface oceanic circulation and the marine environment within the Mid-
917 Cretaceous tethys, , 13(5), 546–559, 1998.
918 Poulsen, C. J., Barron, E. J., Arthur, M. A. and Peterson, W. H.: Response of the mid-
919 Cretaceous global oceanic circulation to tectonic and CO<inf>2</inf> forcings,
920 Paleoceanography, 16(6), 576–592, doi:10.1029/2000PA000579, 2001.
921 Poulsen, C. J., Gendaszek, A. S. and Jacob, R. L.: Did the rifting of the Atlantic Ocean cause
922 the Cretaceous thermal maximum?, Geology, 31(2), 115–118, doi:10.1130/0091-
923 7613(2003)031<0115:DTROTA>2.0.CO;2, 2003.
924 Poulsen, C. J., Pollard, D. and White, T. S.: General circulation model simulation of the δ18O
925 content of continental precipitation in the middle Cretaceous: A model-proxy comparison,
926 Geology, 35(3), 199–202, doi:10.1130/G23343A.1, 2007.
927 Pucéat, E., Lécuyer, C., Donnadieu, Y., Naveau, P., Cappetta, H., Ramstein, G., Huber, B. T.
928 and Kriwet, J.: Fish tooth δ18O revising Late Cretaceous meridional upper ocean water
929 temperature gradients, Geology, 35(2), 107–110, doi:10.1130/G23103A.1, 2007.
930 Robinson, S. A., Dickson, A. J., Pain, A., Jenkyns, H. C., O'Brien, C. L., Farnsworth, A. and
931 Lunt, D. J.: Southern Hemisphere sea-surface temperatures during the Cenomanian-Turonian:
932 Implications for the termination of Oceanic Anoxic Event 2, Geology, 47(2), 131–134,
933 doi:10.1130/G45842.1, 2019.
934 Rose, B. E. J. and Ferreira, D.: Ocean heat transport and water vapor greenhouse in a warm
935 equable climate: A new look at the low gradient paradox, J. Clim., 26(6), 2117–2136,
936 doi:10.1175/JCLI-D-11-00547.1, 2013.

https://doi.org/10.5194/cp-2019-166
Preprint. Discussion started: 14 January 2020

Royer, D. L.: Atmospheric CO2 and O2 During the Phanerozoic: Tools, Patterns, and Impacts, 2nd ed., Elsevier Ltd., 2013.

Royer, D. L., Berner, R. A. and Park, J.: Climate sensitivity constrained by CO2 concentrations over the past 420 million years, Nature, 446(7135), 530–532, doi:10.1038/nature05699, 2007.

Sandler, A. and Harlavan, Y.: Early diagenetic illitization of illite-smectite in Cretaceous sediments (Israel): evidence from K-Ar dating, Clay Miner., 41(2), 637–658, doi:10.1180/0009855064120210, 2006.

Sarr, A. C., Sepulchre, P. and Husson, L.: Impact of the Sunda Shelf on the Climate of the Maritime Continent, J. Geophys. Res. Atmos., doi:10.1029/2018JD029971, 2019.

Schmidt, G. A. and Mysak, L. A.: Can increased poleward oceanic heat flux explain the warm Cretaceous climate?, Paleoceanography, 11(5), 579–593, doi:10.1029/96PA01851, 1996.

Sellers, P. ., Bounoua, L., Collatz, G. J., Randall, D. A., Dazlich, D. A., Los, S. O., Berry, J. A., Fung, I., Tucker, C. J., Field, C. B. and Jensen, T. G.: Comparison of Radiative and Physiological Effects of Doubled Atmospheric CO2 on Climate, , 1402–1406, 1996.

Sellwood, B. W., Price, G. D. and Valdest, P. J.: Cretaceous temperatures, , 370(August), 453–455, 1994.

Sewall, J. O., Van De Wal, R. S. W., Van Der Zwan, K., Van Oosterhout, C., Dijkstra, H. A. and Scotese, C. R.: Climate model boundary conditions for four Cretaceous time slices, Clim. Past, 3(4), 647–657, doi:10.5194/cp-3-647-2007, 2007.

Simmons, H. L., Jayne, S. R., St. Laurent, L. C. and Weaver, A. J.: Tidally driven mixing in a numerical model of the ocean general circulation, Ocean Model., 6(3–4), 245–263, doi:10.1016/S1463-5003(03)00011-8, 2004.

Spicer, R. A. and Herman, A. B.: The Late Cretaceous environment of the Arctic: A quantitative reassessment based on plant fossils, Palaeogeogr. Palaeoclimatol. Palaeoecol., 295(3–4), 423–442, doi:10.1016/j.palaeo.2010.02.025, 2010.

Swingedouw, D., Rodehacke, C. B., Olsen, S. M., Menary, M., Gao, Y., Mikolajewicz, U. and Mignot, J.: On the reduced sensitivity of the Atlantic overturning to Greenland ice sheet melting in projections: a multi-model assessment, Clim. Dyn., 44(11–12), 3261–3279, doi:10.1007/s00382-014-2270-x, 2015.

Swingedouw, D., Mignot, J., Guilyardi, E., Nguyen, S. and Ormières, L.: Tentative reconstruction of the 1998–2012 hiatus in global temperature warming using the IPSL–CM5A–LR climate model, Comptes Rendus - Geosci., 349(8), 369–379, doi:10.1016/j.crte.2017.09.014, 2017.

https://doi.org/10.5194/cp-2019-166
Preprint. Discussion started: 14 January 2020

971 Tabor, C. R., Poulsen, C. J., Lunt, D. J., Rosenbloom, N. A., Otto-Bliesner, B. L., Markwick,
972 P. J., Brady, E. C., Farnsworth, A. and Feng, R.: The cause of Late Cretaceous cooling: A
973 multimodel-proxy comparison, Geology, 44(11), 963–966, doi:10.1130/G38363.1, 2016.
974 Tagliabue, A., Bopp, L., Dutay, J. C., Bowie, A. R., Chever, F., Jean-Baptiste, P., Bucciarelli,
975 E., Lannuzel, D., Remenyi, T., Sarthou, G., Aumont, O., Gehlen, M. and Jeandel, C.:
976 Hydrothermal contribution to the oceanic dissolved iron inventory, Nat. Geosci., 3(4), 252–
977 256, doi:10.1038/ngeo818, 2010.
978 Tan, N., Ramstein, G., Dumas, C., Contoux, C., Ladant, J. B., Sepulchre, P., Zhang, Z. and
979 De Schepper, S.: Exploring the MIS M2 glaciation occurring during a warm and high
980 atmospheric CO2Pliocene background climate, Earth Planet. Sci. Lett., 472, 266–276,
981 doi:10.1016/j.epsl.2017.04.050, 2017.
982 Turgeon, S. C. and Creaser, R. A.: Cretaceous oceanic anoxic event 2 triggered by a massive
983 magmatic episode, , 454(July), doi:10.1038/nature07076, 2008.
984 Upchurch, G. R.: Vegetation-atmosphere interactions and their role in global warming during
985 the latest Cretaceous, Philos. Trans. R. Soc. B Biol. Sci., 353(1365), 97–112,
986 doi:10.1098/rstb.1998.0194, 1998.
987 Upchurch, G. R., Kiehl, J., Shields, C., Scherer, J. and Scotese, C.: Latitudinal temperature
988 gradients and high-latitude temperatures during the latest Cretaceous: Congruence of geologic
989 data and climate models, Geology, 43(8), 683–686, doi:10.1130/G36802.1, 2015.
990 Valcke, S., Budich, R., Carter, M., Guilyardi, E., Lautenschlager, M., Redler, R. and
991 Steenman-clark, L.: The PRISM software framework and the OASIS coupler, , 5(September
992 2014), 2001–2004, 2006.
993 Vandermark, D., Tarduno, J. A. and Brinkman, D. B.: A fossil champsosaur population from
994 the high Arctic: Implications for Late Cretaceous paleotemperatures, Palaeogeogr.
995 Palaeoclimatol. Palaeoecol., 248(1–2), 49–59, doi:10.1016/j.palaeo.2006.11.008, 2007.
996 Veizer, J., Godderis, Y. and François, L. M.: Evidence for decoupling of atmospheric CO 2
997 and global climate during the Phanerozoic eon, Nature, 408(6813), 698–701,
998 doi:10.1038/35047044, 2000.
999 Wang, Y., Huang, C., Sun, B., Quan, C., Wu, J. and Lin, Z.: Paleo-CO2 variation trends and
1000 the Cretaceous greenhouse climate, Earth-Science Rev., 129, 136–147,
1001 doi:10.1016/j.earscirev.2013.11.001, 2014.
1002 Wilson, M. F. and Henderson-sellers, A.: LBA Regional Vegetation and Soils, 1-Degree
1003 (Wilson and Henderson-Sellers), , doi:10.3334/ORNLDAAC/687, 2003.
1004 Woillez, M. N., Levavasseur, G., Daniau, A. L., Kageyama, M., Urrego, D. H., Sánchez-

https://doi.org/10.5194/cp-2019-166
Preprint. Discussion started: 14 January 2020

1005 Goñi, M. F. and Hanquiez, V.: Impact of precession on the climate, vegetation and fire
1006 activity in southern Africa during MIS4, Clim. Past, 10(3), 1165–1182, doi:10.5194/cp-10-
1007 1165-2014, 2014.
1008 Zhou, J., Poulsen, C. J., Rosenbloom, N., Shields, C. and Briegleb, B.: Vegetation-climate
1009 interactions in the warm mid-Cretaceous, Clim. Past, 8(2), 565–576, doi:10.5194/cp-8-565-
1010 2012, 2012.
1011 Zhu, J., Poulsen, C. J. and Tierney, J. E.: Simulation of Eocene extreme warmth and high
1012 climate sensitivity through cloud feedbacks, Sci. Adv., 5(9), eaax1874,
1013 doi:10.1126/sciadv.aax1874, 2019.
1014 Zobler, L.: Global Soil Types, 1-Degree Grid (Zobler), , doi:10.3334/ORNLDAAC/418,
1015 1999.
1016
1017
1018